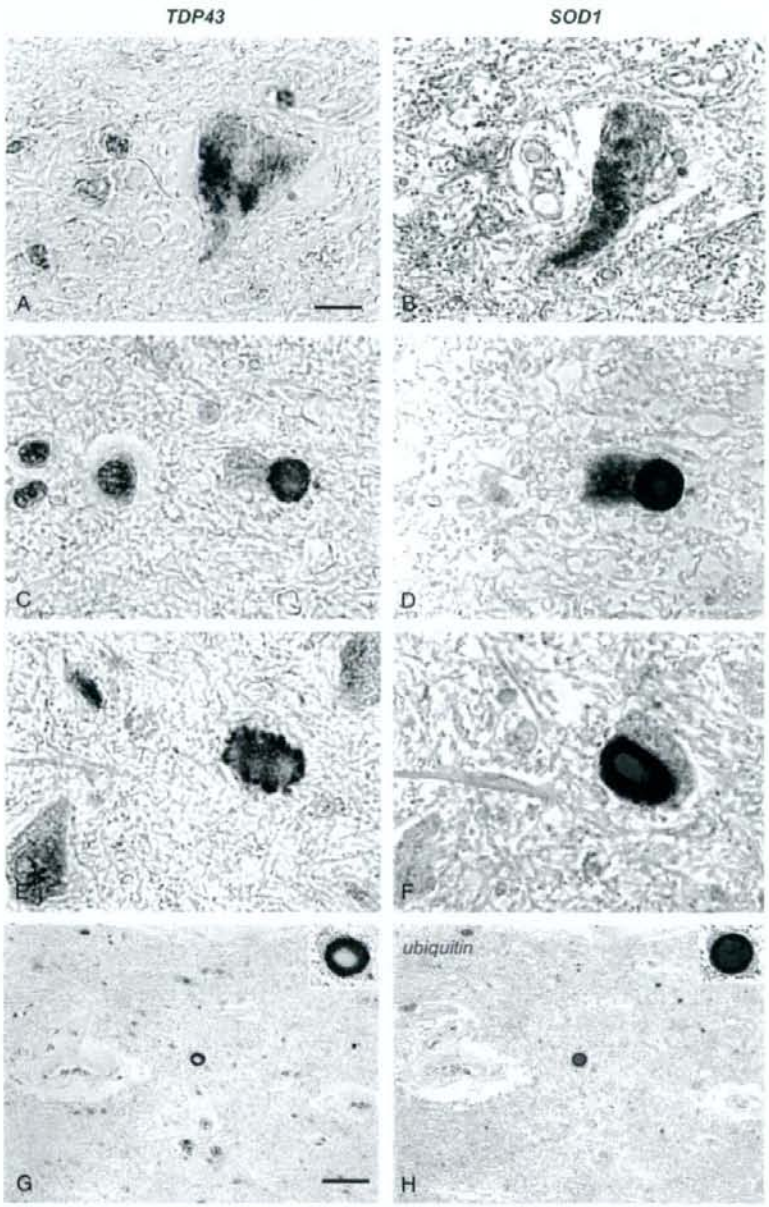

FIGURE 2. Colocalization of TAR DNA binding protein (TDP) and superoxide dismutase 1 (SOD1) in neurons of an amyotrophic lateral sclerosis 1 (C111Y) patient. **(A, B)** Heterogeneous cytoplasmic staining patterns for TDP **(A)** and for SOD1 **(B)**. The nucleus is TDP negative. **(C–F)** Neuronal inclusions are positive for TDP **(C, E)** and SOD1 **(D, F)**. **(G, H)** The halo portion of a Lewy body–like hyaline inclusion (LBHI) is stained strongly for TDP **(G)** and ubiquitin **(H)**. The upper panels are high-magnification views of each LBHI. Immunohistochemistry: **(A, C, E, G)** = TDP; **(B, D, F)** = SOD1; **(H)** = ubiquitin. **(B, D, F,** and **H)** are adjacent serial sections of **(A, C, E,** and **G)**, respectively. Scale bars = **(A–F)** 10 μm; **(G, H)** 50 μm; insets in **(G, H)** = 16 μm.

an aggregation pattern (Figs. 2A–F). The TDP and ubiquitin were also colocalized in inclusions (Figs. 2G, H). Patients ALS1-2 (30) and ALS1-3 (31) possessed the same SOD1 mutation; TDP-IR of the nuclei was weaker in Patient ALS1-3,who had more LBHIs than Patient ALS1-2. The TDP-IR of some of the LBHIs observed in these patients was weak, but stronger than that in most of the nuclei (Fig. 3A). Colocalization of TDP and SOD1 was demonstrated in LBHIs in serial sections (Figs. 3A, B). The LBHIs were scarce in other ALS1 patients. Although TDP-IR was retained in the nuclei of most of the residual neurons in Patients ALS1-4 (G37R) (32) and ALS1-5 (L126S) (33), there were a few neurons with TDP-negative nuclei and cytoplasm. The TDP-negative nuclei were atrophic or deformed (Fig. 3D), whereas most of the TDP-positive nuclei were circular (Fig. 3F). In ALS1 patients, there was no apparent relationship between nuclear TDP-IR and disease duration. The SMI31-positive conglomerate inclusions (Fig. 3E) in Patients ALS1-5 and ALS1-6 were mostly TDP negative (Fig. 3F) or had only very faint staining (Fig. 3D).

G93A Mice

In normal littermates, TDP-IR was found in the neurons and some glia in the gray matter (Fig. 4A); the white matter was negative for TDP. In G1L mice, the nuclei of neurons and reactive astrocytes were stained for TDP. The

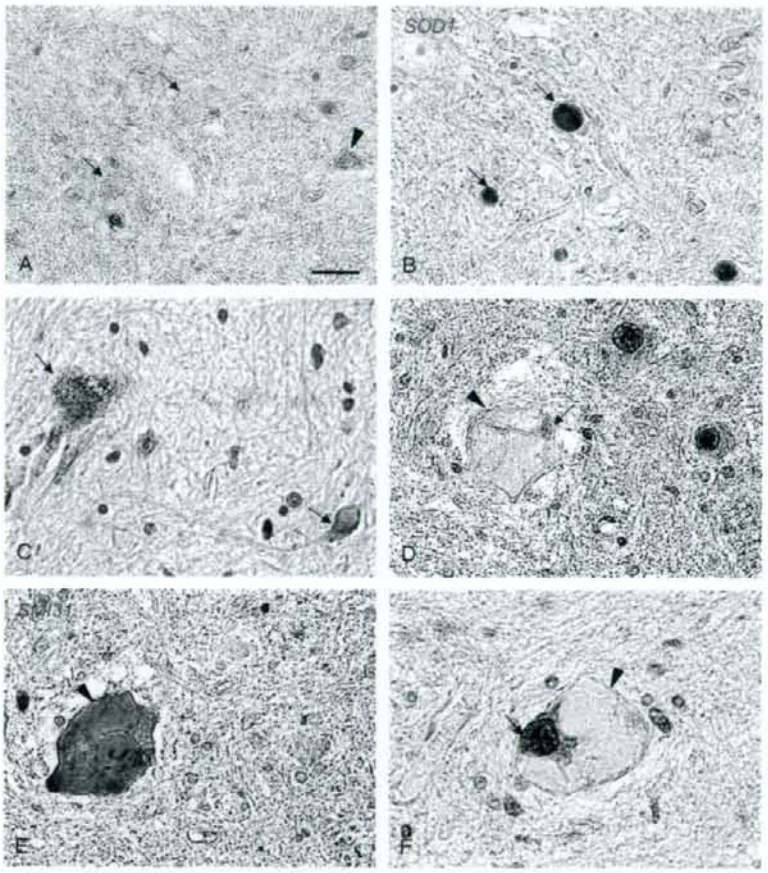

FIGURE 3. TAR DNA binding protein (TDP) staining patterns in the other amyotrophic lateral sclerosis 1 patients. **(A, B)** Superoxide dismutase 1 (SOD1)–positive Lewy body–like hyaline inclusions **(B)** are weakly stained (left, arrow) and very faintly stained (right, arrow) for TDP **(A)**. There is mislocalization in a small neuron (arrowhead) in **(A)**. **(C)** The neuron cytoplasm is diffusely stained for TDP (arrows). **(D, E)** A conglomerate inclusion is positive for SMI31 (**[E]** arrowhead) and is negative for TDP (**[D]** arrowhead). The nucleus (**[D]** arrow) is atrophic and deformed. **(F)** The TDP-positive nucleus (arrow) in a neuron containing a TDP-negative conglomerate inclusion (arrowhead) appears round and intact. Immunohistochemistry: **(A, C, D, F)** = TDP; **(B)** = SOD1; **(E)** = phosphorylated neurofilament (SMI31). **(B)** and **(E)** are serial sections of **(A)** and **(D)**, respectively. Scale bar = 20 μm.

cytoplasm of a few anterior horn cells showed a punctate TDP staining pattern, but most of the neuron nuclei were TDP positive (Figs. 4E, 5C). Neurons with TDP-negative nuclei and TDP-positive cytoplasm were rare (Fig. 4B). The TDP-positive inclusions and neurites were numerous (Figs. 4C, 5A–D), and the nuclear TDP-IR of these cells was weak (Fig. 5A). Some vacuoles were also stained for TDP (Fig. 4C). Colocalization of TDP and SOD1 was also detected in LBHIs in serial sections (Figs. 4C, D). Nuclear TDP-IR varied widely from mouse to mouse (Stages 1–4, Figs. 5A–D). In G1L mice showing a rapid clinical course and prominent LBHI-formation, nuclear TDP-IR was weak (Stage 1, Figs. 5A, E), whereas G1L mice showing a slow clinical course and less LBHI formation had strong nuclear TDP-IR (Stage 4, Figs. 5D, F). In Stage 4 mice, most of the nuclei were strongly positive and circular, but some weakly stained nuclei were atrophic or deformed (Fig. 4E). In G1H mice with a rapid disease course, TDP-IR of the neurons was weak, and nearly all LBHIs in the lumbar spinal cord were negative for TDP (Fig. 4F).

Statistical Analysis

The numbers of TDP-positive inclusions in neurons and glia were significantly lower in SALS patients with a

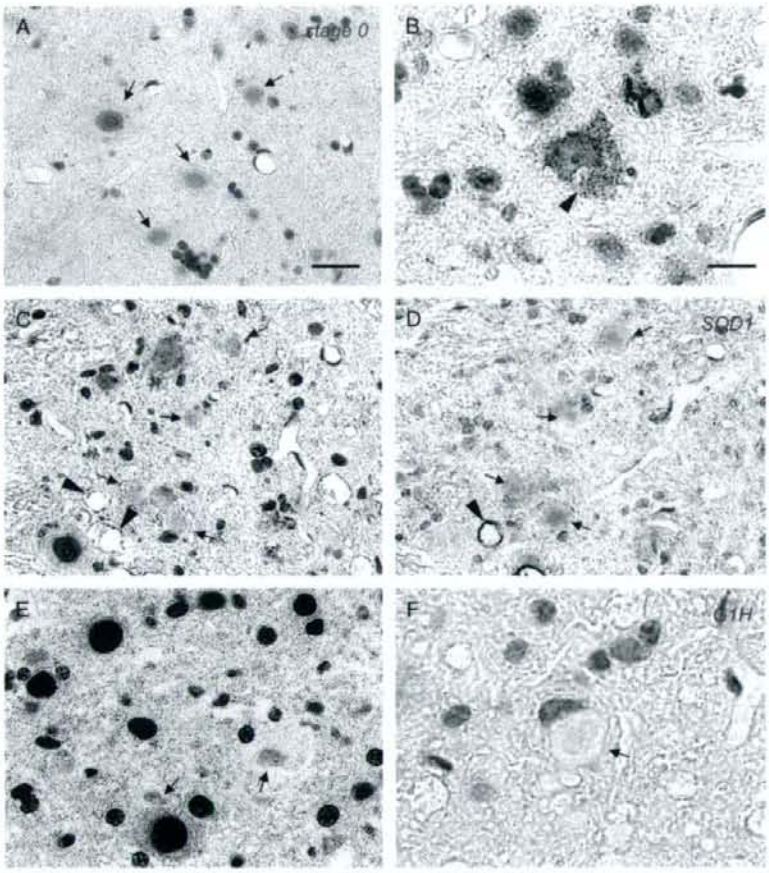

FIGURE 4. TAR DNA binding protein (TDP) pathology in G93A mice. **(A)** Nuclei in large neurons in a normal littermate (arrows) are TDP positive; their nucleoli are not stained. **(B–E)** G1L mice. **(B)** A degenerated neuron containing small vacuoles (arrowhead) in the cytoplasm has a TDP-negative nucleus and TDP-positive cytoplasm. **(C, D)** There are numerous Lewy body-like hyaline inclusions (LBHIs) that are TDP positive **(C)** and superoxide dismutase 1 (SOD1) **(D)** (arrows). Some vacuoles that are SOD1 positive **(D)** are partly stained for TDP (**C**, arrowheads). **(E)** Most of the nuclei in the neurons are strongly positive for TDP. A few nuclei that are stained only weakly (arrows) are atrophic and deformed. **(F)** The LBHI in the lumbar cord of the G1H mouse stains extremely faintly for TDP (arrow). **(A)** Normal littermate (Stage 0), **(B–E)** G1L mice, **(B–D)** Stage 3, **(E)** Stage 4, **(F)** G1H mouse. Immunohistochemistry for TDP **(A–C, E, F)** and SOD1 **(D)**. **(D)** is a serial section of **(C)**. Scale bars = (**A, C–E**) 50 μm; **(B, F)** 20 μm.

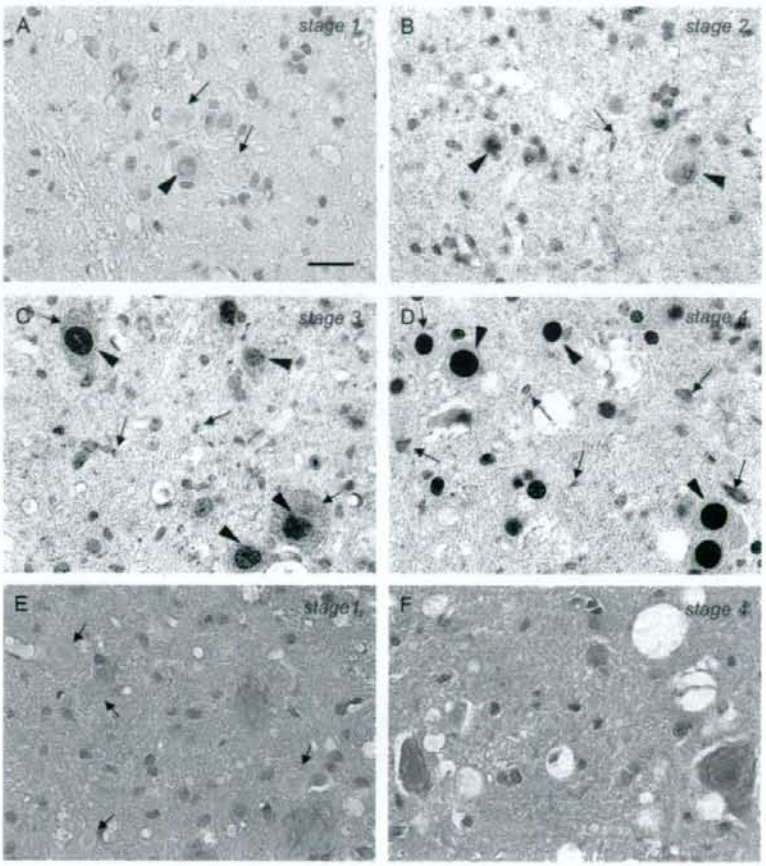

FIGURE 5. Four stages of TAR DNA binding protein (TDP) immunoreactivity in spinal cord neuron nuclei of G1L mice. (**A**) In Stage 1, nuclear immunoreactivity (arrowhead) is weak. Lewy body-like hyaline inclusions (LBHIs) (arrows) are only faintly stained or negative. (**B**) In Stage 2, nuclear immunoreactivity of neuron nuclei (arrowheads) is similar to that of normal littermates (Fig. 4A). Neurites or tiny vacuoles (arrow) also show immunoreactivity. (**C**) Immunoreactivity in Stage 3 in most of the nuclei (arrowheads) is stronger than in the normal control, but less than in Stage 4. There is diffuse and punctate cytoplasm staining and immunoreactivity in neurites (arrows). (**D**) Nuclear immunoreactivity in Stage 4 is very strong (arrowheads), and there are numerous TDP-positive neurites (arrows). (**E**) Prominent LBHIs (arrows) are evident in a Stage 1 mouse. (**F**) In a Stage 4 mouse, there are many vacuoles detected, but there is no LBHI formation. Immunohistochemistry for TDP (**A–D**); hematoxylin and eosin stain (**E, F**). Scale bar = 50 μm.

slow course than in those with a rapid course (Wilcoxon rank sum test: neuronal inclusions, $p = 0.0002$; glial inclusions, $p = 0.0002$). The numbers of large neurons (>37 μm) were also lower in SALS patients with a slow course than in those with a rapid course, although the level of significance ($p = 0.0264$) was lower than that for TDP-positive inclusions. The relationships among the numbers of large neurons, and TDP-positive inclusions in neurons and glia were not significant in SALS patients as a whole (Spearman correlation coefficient with 95% CI).

In G1L mice, the TDP-IR stage was positively correlated with life span (Spearman correlation coefficient with 95% CI, $r = 0.77$; 95% CI, 0.22–0.95) and negatively correlated with the formation of LBHIs ($r = -0.87$; 95% CI, −0.97 to −0.47). The correlation between life span and the number of LBHIs was also high ($r = -0.64$; 95% CI, −0.92 to 0.04). A cumulative probability plot of age at the end stage (Fig. 6) showed a higher value for the group with strong TDP-IR (Stages 3 and 4) than for those with weak TDP-IR (Stages 1 and 2); age at the end stage in the strong TDP-IR group was significantly greater than that in the weak TDP-IR group (Kolmogorov-Smirnov test, $p = 0.015$).

DISCUSSION

The TDP mislocalization from the nucleus to the cytoplasm was previously considered to be a disease-specific

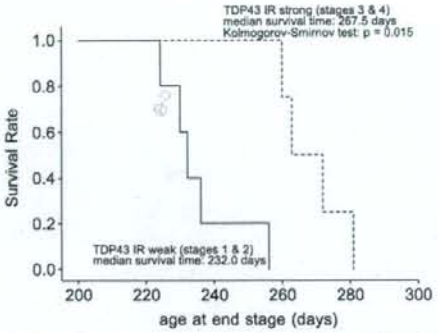

FIGURE 6. Kolmogorov-Smirnov test of the weak TAR DNA binding protein immunoreactivity (TDP-IR) groups (Stages 1 and 2) and strong TDP-IR groups (Stages 3 and 4) of G1L mice. Age at end stage in the TDP-IR strong group was significantly greater than that in the TDP-IR weak group ($p = 0.015$).

change not present in ALS1. Here, we analyzed TDP pathology in SALS and ALS1 patients and in ALS1 model mice. Our data suggest that the level of expression of TDP in the nucleus is associated with the clinical course and neurodegenerative changes in SALS patients and in ALS1 model mice.

Our observation that diffuse staining pattern was frequently observed in the cytoplasm of large neurons in SALS patients with rapid clinical courses showing mild neuronal loss suggests that TDP mislocalization starts gradually in the early phase of neurodegeneration. Most of the TDP-positive inclusions were found in atrophic neurons and glia, suggesting that the inclusions appeared later. Because no extracellular TDP-positive inclusions were apparent, neuronal TDP-positive inclusions likely disappear along with the death of the neurons.

In contrast, in SALS patients with slow clinical courses, no neurons with a diffuse TDP staining pattern in the cytoplasm were found, and TDP-positive inclusions in both neurons and glia were significantly less frequently found. Because relationships among the numbers of large neurons, those of TDP-positive inclusions in neurons, and those of TDP-positive inclusions in glia were not significant, the rarity of TDP pathology in SALS patients with a slow clinical course might not necessarily have resulted from severe neurodegeneration. The TDP pathology might be associated with a rapid clinical course in SALS. The influence of TDP-43 on the disease would then be less marked in SALS patients with a slow clinical course than in those with a rapid clinical course.

Previous studies have shown that LBHIs are not stained for TDP in ALS1 patients (16, 17, 26) and G1H mice (26).

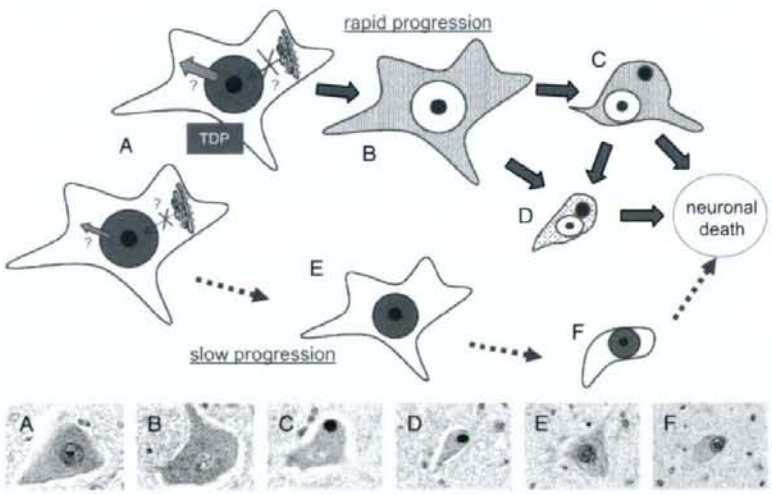

FIGURE 7. Hypothetical course of neuronal degeneration associated with changes in nuclear TAR DNA binding protein (TDP) expression in sporadic amyotrophic lateral sclerosis (SALS). **(A)** A morphologically normal neuron is subjected to an insult associated with a disturbance of TDP nuclear trafficking. The upper neuron diagrammed, from a patient with SALS, showing a rapid clinical course has marked disturbance of TDP nuclear trafficking, whereas the lower diagrammed neuron from a patient with SALS showing a slow clinical course, is only mildly affected. **(B–D)** Images show degenerating neurons at the time of rapid disease progression. **(B)** Early occurrence of TDP redistribution, i.e. low expression in nuclei and high expression in cytoplasm. **(C)** Later occurrence of cytoplasmic TDP aggregate in an atrophic neuron. **(D)** Similar aggregate of cytoplasmic TDP in a more degenerative neuron than that in **(C)**. **(E, F)** Images represent degenerative neurons at the time of slow disease progression. **(E)** Preservation of a high level of TDP expression in the nucleus of an atrophic neuron. **(F)** Successive maintenance of a high level of TDP expression in the nucleus of a more degenerative neuron. The lower 6 photographs are from SALS patients showing a rapid clinical course **(A–D)** and a slow course **(E, F)**, which correspond to the diagrammatic illustrations for each letter.

On the other hand, mislocalization of TDP to the cytoplasm in ALS1 cases (A4T, I113T) has been reported by Robertson et al (26). In the present study, TDP-positive LBHIs were clearly demonstrated in 1 ALS1 patient showing a slow disease progression, and in G1L mice, which also show slower disease progression than G1H mice. The ALS1 patients with TDP-negative LBHIs reported by Tan et al (17) showed very rapid progression within less than 1 year, and another ALS1 patient with TDP-negative LBHIs reported by Robertson et al (26) also showed rapid progression within 2 years. The difference in TDP immunoreactivity of LBHIs among ALS1 cases or between the 2 kinds of G93A mice might be a result of the difference in the clinical course or speed of SOD1 aggregation (34). The difference in morphology between TDP-positive inclusions in ALS1-1 and G1L mice and those in SALS patients would be caused by trapping of TDP-43 by SOD1 aggregation or LBHIs. The colocalization of TDP and SOD1 in LBHIs also suggests a biological relationship between SOD1 and TDP, although the specifics of that relationship are unclear.

Ayala et al (11) reported that loss of TDP in vitro results in nuclear dysmorphism, misregulation of the cell cycle, and apoptosis. Because the TDP-IR stage was positively correlated with life span in G1L mice, nuclei with low TDP-IR were atrophic and deformed in G1L mice and ALS1 patients, and an absence of TDP in the nucleus (such as that occurring through mislocalization) was frequently observed in SALS patients with a rapid clinical course, a high level of expression of nuclear TDP may play a protective role in neurons exposed to various insults. Because TDP-IR in the nucleus was inversely correlated with LBHI formation in G1L mice, TDP might have a suppressive effect on LBHI formation or toxic aggregation of SOD1, possibly through changes in the transcription and splicing of unknown genes (7, 8).

We hypothesized that rapid disease progression resulting from some insult to neurons might lead to disturbance of TDP nuclear trafficking (Fig. 7A) (35). Redistribution of TDP, with a low level of expression in the nucleus and a high level in the cytoplasm (Fig. 7B), occurs first, and cytoplasmic TDP later forms aggregates in the atrophic neurons (Figs. 7C, D). In contrast, neurons that succeed in maintaining a high level of expression of nuclear TDP (36) because of a slow shift of TDP (Fig. 7A, lower) show rather slower degeneration, and the disease progresses more slowly (Figs. 7E, F). It will be important to investigate the mechanism responsible for regulating the nuclear expression level of TDP, as this might yield a new strategy for treating not only ALS, but also other neurodegenerative disorders, including frontotemporal lobar degeneration.

ACKNOWLEDGMENTS

The authors thank T. Hamasaki and T. Sugimoto for their expert assistance with statistical analyses, and R. Yasui for technical assistance.

REFERENCES

1. Deng H-X, Hentati A, Tainer JA, et al. Amyotrophic lateral sclerosis and structural defects in Cu/Zn superoxide dismutase. Science 1993;261: 1047–51
2. Rosen DR, Siddique T, Patterson D, et al. Mutations in Cu/Zn superoxide dismutase gene are associated with familial amyotrophic lateral sclerosis. Nature 1993;362:59–62
3. Kato S. Amyotrophic lateral sclerosis models and human neuropathology: Similarities and differences. Acta Neuropathol 2008;115:97–114
4. Hadano S, Hand CK, Osuga H, et al. A gene encoding a putative GTPase regulator is mutated in familial amyotrophic lateral sclerosis 2. Nat Genet 2001;29:166–73
5. Yang Y, Hentati A, Deng HX, et al. The gene encoding alsin, a protein with three guanine-nucleotide exchange factor domains, is mutated in a form of recessive amyotrophic lateral sclerosis. Nat Genet 2001;29: 160–65
6. Buratti E, Brindisi A, Giombi M, et al. TDP-43 binds heterogenous nuclear ribonucleoprotein A/B through its C-terminal tail. J Biol Chem 2005;280:37572–84
7. Ayala YM, Pantano S, D'Ambrogio A, et al. Human, *Drosophila*, and *C. elegans* TDP43: Nucleic acid binding properties and splicing regulatory function. J Mol Biol 2005;348:575–88
8. Wang HY, Wang IF, Bose J, Shen CKJ. Structural diversity and functional implications of the eukaryotic *TDP* gene family. Genomics 2004;83:130–39
9. Buratti E, Baralle FE. Characterization and functional implications of the RNA binding properties of nuclear factor TDP-43, a novel splicing regulator of CFTR exon9. J Biol Chem 2001;276:36337–43
10. Mercado PA, Ayala YM, Romano M, et al. Depletion of TDP43 overrides the need for exonic and intronic splicing enhancers in the human apoA-II gene. Nucleic Acids Res 2005;33:6000–10
11. Ayala YM, Misteli T, Baralle FE. TDP-43 regulates retinoblastoma protein phosphorylation through the repression of cyclin-dependent kinase 6 expression. Proc Natl Acad Sci U S A 2008;105:3785–89
12. Kato S, Takikawa M, Nakashima K, et al. New consensus research on neuropathological aspects of familial amyotrophic lateral sclerosis with superoxide dismutase 1 (SOD1) gene mutations: Inclusions containing SOD1 in neurons and astrocytes. Amyotroph Lateral Scler Other Motor Neuron Disord 2000;1:163–84
13. Arai T, Hasegawa M, Akiyama H, et al. TDP-43 is a component of ubiquitin-positive tau-negative inclusions in frontotemporal lobar degeneration and amyotrophic lateral sclerosis. Biochem Biophys Res Commun 2006;351:602–11
14. Neumann M, Sampathu DM, Kwong LK, et al. Ubiquitinated TDP-43 in frontotemporal lobar degeneration and amyotrophic lateral sclerosis. Science 2006;314:130–33
15. Dickson DW, Josephs KA, Amador-Ortiz C. TDP-43 in differential diagnosis of motor neuron disorders. Acta Neuropathol 2007;114:71–79
16. Mackenzie IRA, Bigio EH, Ince PG, et al. Pathological TDP-43 distinguishes sporadic amyotrophic lateral sclerosis from amyotrophic lateral sclerosis with SOD1 mutations. Ann Neurol 2007;61:427–34
17. Tan C-F, Eguchi H, Tagawa A, et al. TDP-43 immunoreactivity in neuronal inclusions in familial amyotrophic lateral sclerosis with or without *SOD1* gene mutation. Acta Neuropathol 2007;113:535–42
18. Gitcho MA, Baloh RH, Chakraverty S, et al. TDP-43 A315T mutation in familial motor neuron disease. Ann Neurol 2008;63:535–38
19. Sreedharan J, Blair IP, Tripathi VB, et al. TDP-43 mutations in familial and sporadic amyotrophic lateral sclerosis. Science 2008;319: 1668–72
20. Cairns NJ, Neumann M, Bigio EH, et al. TDP-43 in familial and sporadic frontotemporal lobar degeneration with ubiquitin inclusions. Am J Pathol 2007;171:227–40
21. Amador-Ortiz C, Lin W-L, Ahmed Z, et al. TDP-43 immunoreactivity in hippocampal sclerosis and Alzheimer's disease. Ann Neurol 2007;6: 435–45
22. Nakashima-Yasuda H, Uryu K, Robinson J, et al. Co-morbidity of TDP-43 proteinopathy in Lewy body–related diseases. Acta Neuropathol 2007;114:221–29
23. Freeman SH, Spires-Jones TDP, Hyman BT, et al. TAR-DNA binding protein 43 in Pick disease. J Neuropathol Exp Neurol 2008;67:62–67
24. Lee EB, Lee M-Y, Trojanowski JQ, Neumann M. TDP-43 immunoreactivity in anoxic, ischemic and neoplastic lesions of the central nervous system. Acta Neuropathol 2007;115:305–11
25. Sanelli T, Xiao S, Horne P, et al. Evidence that TDP-43 is not the major ubiquitinated target within the pathological inclusions of amyotrophic lateral sclerosis. J Neuropathol Exp Neurol 2007;66:1147–53

26. Robertson J, Sanelli T, Xiao S, et al. Lack of TDP-43 abnormalities in mutant SOD1 transgenic mice shows disparity with ALS. Neurosci Lett 2007;420:128–32
27. Dal Canto MC, Gurney ME. A low expressor line of transgenic mice carrying a mutant *SOD1* gene develops pathological changes that most closely resemble those in human amyotrophic lateral sclerosis. Acta Neuropathol 1997;93:537–50
28. Parent A, Carpenter MB. *Carpenter's Human Neuroanatomy, 9th ed.* Philadelphia, PA: Lippincott, Williams &Wilkins, 1996
29. Sumi H, Nagano S, Fujimura H, et al. Inverse correlation between the formation of mitochondria-derived vacuoles and Lewy body–like hyaline inclusions in G93A superoxide dismutase–transgenic mice. Acta Neuropathol 2006;112:52–63
30. Kategawa J, Fujimura H, Ogawa Y, et al. A clinicopathological study of familial amyotrophic lateral sclerosis associated with two pair deletion in the copper/zinc superoxide dismutase (SOD1) gene. Acta Neuropathol (Berl) 1997;94:617–22
31. Kato S, Shimoda M, Watanabe Y, et al. Familial amyotrophic lateral sclerosis with a two base pair deletion in superoxide dismutase 1 (SOD1): Gene multisystem degeneration with intracytoplasmic hyaline inclusions in astrocytes. J Neuropathol Exp Neurol 1996;55:1089–101
32. Inoue K, Fujimura H, Ogawa Y, et al. Familial amyotrophic lateral sclerosis with a point mutation (G37R) of the superoxide dismutase 1 gene: A clinicopathological study. Amyotroph Lateral Scler Other Motor Neuron Disord 2002;3:244–47
33. Inoue K, Fujimura H, Toyooka K, et al. Familial amyotrophic sclerosis with L126S mutation of Cu/Zn superoxide dismutase gene. Pathological study of two cases [Abstract]. J Neurol 2006;235:120
34. Sato T, Nakanishi T, Yamamoto Y, et al. Rapid disease progression is correlated with instability of mutant SOD1 in familial ALS. Neurology 2006;65:1954–57
35. Winton MJ, Igaz LM, Wong MM, et al. Disturbance of nuclear and cytoplasmic Tar DNA binding protein (TDP-43) induces disease-like redistribution, sequestration and aggregate formation. J Biol Chem 2008; 283:13302–9
36. Wang IF, Chang HY, James Shen CK. TDP-43, the signature protein of FTLD-U, is a neuronal activity-responsive factor. J Neurochem 2008; 105:797–806

Journal of Neuroscience Research 86:2512–2523 (2008)

Accumulation of Chondroitin Sulfate Proteoglycans in the Microenvironment of Spinal Motor Neurons in Amyotrophic Lateral Sclerosis Transgenic Rats

Hideki Mizuno, Hitoshi Warita,* Masashi Aoki, and Yasuto Itoyama

Division of Neurology, Department of Neuroscience, Tohoku University Graduate School of Medicine and Tohoku University Hospital ALS Center, Sendai, Japan

Chondroitin sulfate proteoglycans (CSPGs) are the major components of extracellular matrix in the central nervous system. In the spinal cord under various types of injury, reactive gliosis emerges in the lesion accompanied by CSPG up-regulation. Several types of CSPG core proteins and their side chains have been shown to inhibit axonal regeneration in vitro and in vivo. In the present study, we examined spatiotemporal expression of CSPGs in the spinal cord of transgenic (Tg) rats with His46Arg mutation in the *Cu/Zn superoxide dismutase* gene, a model of amyotrophic lateral sclerosis (ALS). Immunofluorescence disclosed a significant up-regulation of neurocan, versican, and phosphacan in the ventral spinal cord of Tg rats compared with age-matched controls. Notably, Tg rats showed progressive and prominent accumulation of neurocan even at the presymptomatic stage. Immunoblotting confirmed the distinct increase in the levels of both the full-length neurocan and their fragment isoforms. On the other hand, the up-regulation of versican and phosphacan peaked at the early symptomatic stage, followed by diminishment at the late symptomatic stage. In addition, double immunofluorescence revealed a colocalization between reactive astrocytes and immunoreactivities for neurocan and phosphacan, especially around residual large ventral horn neurons. Thus, reactive astrocytes are suggested to be participants in the CSPG accumulation. Although the possible neuroprotective involvement of CSPG remains to be investigated, the present results suggest that both the reactive astrocytes and the differential accumulation of CSPGs may create a nonpermissive microenvironment for neural regeneration in neurodegenerative diseases such as ALS.

Key words: amyotrophic lateral sclerosis; chondroitin sulfate proteoglycan; microenvironment; SOD1; transgenic rat

Amyotrophic lateral sclerosis (ALS) is a relentless and progressive neurodegenerative disease characterized by adult-onset selective loss of motor neurons, which causes skeletal muscle atrophy and weakness, and ultimately death. In approximately 10% of all ALS patients, this condition is familial, mainly with inheritance of an autosomal dominant trait (Haverkamp et al., 1995). Despite clinical and genetic heterogeneity, the pathologies of familial ALS and that of sporadic ALS are similar, suggesting a common pathomechanism. In about 20% of familial ALS families, this disease is linked to mutations in the *Cu/Zn superoxide dismutase* (*SOD1*) gene (Aoki et al., 1993; Rosen et al., 1993). Several lines of transgenic (Tg) rodents ubiquitously overexpressing a mutant *SOD1* transgene recapitulate the ALS phenotype (Gurney et al., 1994; Nagai et al., 2001), whereas *SOD1* knockout mice do not develop motor neuron degeneration (Reaume et al., 1996), indicating a gain of toxicity of mutant SOD1. However, the precise mechanisms of motor neuron death remain to be elucidated (Boillee et al., 2006a).

Recent data from wild-type/mutant SOD1 chimeric mice (Clement et al., 2003) and mice carrying a deletable mutant *SOD1* gene in a cell type-selective manner (Boillee et al., 2006b) demonstrated the noncell-autonomous toxicity of mutant SOD1. These studies have highlighted the involvement of nonneuronal cells, suggesting the significance of the microenvironment surrounding motor neurons. Although no cell-restorative therapy for ALS has been established to date, the possibility of replacing neuronal or nonneuronal cells is of growing interest. Among nonneuronal cells, glial cells constitute the largest cell population in the adult central

Contract grant sponsor: Japanese Ministry of Health, Labor and Welfare; Contract grant number: B: 18790586; Contract grant number: C: 19590977; Contract grant number: 18A-8; Contract grant sponsor: Haruki ALS Research Foundation (to H.W., M.A., Y.I.).

*Correspondence to: Hitoshi Warita, MD, PhD, 1-1 Seiryo-machi, Aoba-ku, Sendai 980-8574, Japan.
E-mail: als@em.neurol.med.tohoku.ac.jp

Received 4 September 2007; Revised 20 December 2007; Accepted 30 January 2008

Published online 25 April 2008 in Wiley InterScience (www.interscience.wiley.com). DOI: 10.1002/jnr.21702

nervous system (CNS). Furthermore, glial cell hypertrophy, proliferation, and accumulation in the affected region are prominent features in CNS damage, including ALS. These glial responses under disease conditions are referred to as *reactive gliosis*, which leads to glial scar formation (Silver and Miller, 2004).

Reactive gliosis is usually accompanied by up-regulation of the regeneration-inhibitory molecules in the extracellular matrix (ECM). This process is believed to create a nonpermissive microenvironment for regeneration. Among the inhibitory molecules, chondroitin sulfate proteoglycans (CSPGs) are the major components in the ECM. Previous reports have demonstrated that CSPGs are inhibitory to neurite outgrowth in vitro and are up-regulated and accumulated after various types of CNS injury in vivo. However, under chronic disease conditions such as neurodegeneration, the expression and distribution of CSPGs have not been investigated previously, except for a few earlier reports (DeWitt et al., 1993, 1994).

The glial role in ALS pathophysiology remains controversial (Neusch et al., 2007), however, the reactive gliosis in the spinal cord has already been reported as a pathological event. Although previous studies have suggested the presence of neural stem/progenitor cells in the intact spinal cord (Gage, 2000; Horner et al., 2000), recent reports have provided controversial results on spontaneous neurogenesis and insufficient evidence for intrinsic regeneration in the spinal cord of mutant *SOD1* Tg mice (Warita et al., 2001; Chi et al., 2006; Liu and Martin, 2006; Guan et al., 2007). These previous studies suggest an absence of inter-/intracellular signals and an inappropriate microenvironment for promoting an endogenous repair mechanism. Thus, substantial interest has recently been paid to the microenvironment, in the context of possible development of cell-restorative therapy with both cell transplantation and endogenous neural progenitor activation (Busch and Silver, 2007).

The present study, therefore, focused on CSPGs such as neurocan, versican, and phosphacan in the microenvironment surrounding degenerating motor neurons. We examined a possible change of the CSPG expression in the adult spinal cord of a rat ALS model and found a significant and differential accumulation of the CSPGs in the neurodegenerative lesion.

MATERIALS AND METHODS

Experimental Animals

Tg rats expressing ALS-associated mutation, His46Arg (H46R) in the human *SOD1* gene (Aoki et al., 1993), were used in this study. They were established in our laboratory, as was the case in our previous report (Nagai et al., 2001). The Tg rats hemizygous for H46R mutation were crossed with wild-type Sprague-Dawley (SD) rats (Slc:SD; Japan SLC, Inc., Shizuoka, Japan) to produce Tg and non-Tg offspring. The Tg progeny were genotyped by polymerase chain reaction amplification of tail DNA with specific primers for exon 4 (Nagai et al., 2001). The H46R Tg rats display an adult-onset motor neuron disease (MND) with later onset, slower progression, and less variability in the phenotype than in the case of Gly93Ala (G93A) transgenic rats (Nagai et al., 2001; Matsumoto et al., 2006). At about 24–25 weeks of age, the Tg rats develop progressive spastic paralysis beginning with a unilateral hindlimb, leading to death about 4 weeks later. The onset of clinical phenotype is delayed by approximately 4–5 weeks in the present Tg rats compared with the original H46R Tg line (Nagai et al., 2001) through multiple passage. The female H46R Tg rats were divided into three experimental groups: presymptomatic (aged 24 weeks, designated *Pre*), early symptomatic (aged 26 weeks, *ES*), and late symptomatic (aged 28 weeks, *LS*). We examined a total of 16 Tg rats and 18 age-matched non-Tg littermates as controls. The rats were housed in a specific pathogen-free animal facility and allowed access to food and water ad libitum. Throughout this study, the animals were handled in the accordance with the *Guide for the care and use of laboratory animals* specified by the Laboratory Animal Welfare Act (National Institutes of Health). All experimental protocols and procedures were approved by the Animal Committee of the Tohoku University Graduate School of Medicine.

Immunofluorescence

The rats were deeply anesthetized with diethyl ether and perfused transcardially with heparinized saline, followed by ice-cold 4% paraformaldehyde in 0.1 M phosphate buffer (PB), pH 7.4. Their lumbar spinal cords (L4–L5) were immediately removed and further fixed by immersion in the same fixative overnight at 4°C, followed by cryoprotection with a series of increasing concentration of sucrose (10% and 20% wt/vol) in 0.1 M PB at 4°C. The tissue samples were embedded in Tissue-Tek O.C.T. compound (Sakura Finetek, Tokyo, Japan) and quickly frozen in 2-methylbutane cooled with liquid nitrogen, then stored at −80°C. Ten-micrometer transverse sections of lumbar spinal cords were cut on a cryostat (CM3050; Leica Instruments, Nussloch, Germany), collected on MAS-coated glass slides (Superfrost; Matsunami Glass, Osaka, Japan), and stored at −80°C. The cryosections were washed in Tris-buffered saline (TBS), pH 7.4. Nonspecific binding was blocked with 5% normal goat serum (Vector Laboratories, Burlingame, CA) and 0.3% Triton X-100 in TBS for 30 min at room temperature (RT). After blocking, the sections were incubated with primary antibodies in the blocking solution overnight at 4°C. We employed the following primary antibodies: rabbit anti-glial fibrillary acidic protein (GFAP) polyclonal IgG (1:1,500; Dako, Glostrup, Denmark), rabbit anti-glutathione S-transferase-π (GST-π) polyclonal IgG (1:1,500; Assay Designs, Ann Arbor, MI), rabbit antineurofilament-H polyclonal IgG (1:1,000; Chemicon International, Temecula, CA), rabbit anti-ionized calcium-binding adapter molecule-1 (Iba-1) polyclonal IgG (1:1,500; Wako Pure Chemical, Osaka, Japan), mouse anti-neurocan monoclonal IgG (1:3,000; clone 650.24; Chemicon International) that is specific for the full-length neurocan core protein and also reacts with the C-terminal fragment, rabbit anti-glycosaminoglycan-α (GAGα) domain of versican V2 (a CNS-specific

splice variant) polyclonal IgG (1:200; Chemicon International) raised against amino acid residues 535–598 of mouse versican, mouse anti-phosphacan/receptor protein tyrosine phosphatase-β (RPTPβ) core protein monoclonal IgM (1:3,000; clone 122.2; Chemicon International), mouse anti-phosphorylated neurofilament-M and -H (pNF) monoclonal IgG (1:1,000; Chemicon International), rabbit anti-ubiquitin (Ub) polyclonal IgG (1:100; Dako), and biotin-conjugated mouse anti-human neuronal protein Hu C/D monoclonal IgG (1:200; Invitrogen, Carlsbad, CA). After extensive rinsing in TBS, the sections were incubated with a combination of appropriate secondary antibodies diluted at 1:500 in an antibody diluent solution (Dako) overnight (4°C). The secondary antibodies used in this study were as follows: goat anti-mouse IgG, anti-mouse IgM, and anti-rabbit IgG conjugated to Alexa Fluor 488 (highly cross-adsorbed; Invitrogen); goat anti-rabbit IgG conjugated to Alexa Fluor 568 (highly cross-adsorbed; Invitrogen); and streptavidin conjugated to Alexa Fluor 647 (Invitrogen). After extensive washing in TBS, the slides were dipped into distilled water and coverslipped with Shandon PermaFluor (Thermo Electron Corporation, Pittsburgh, PA), then kept in the dark at 4°C until analysis. As a negative control, the above-described procedures were repeated without each primary antibody. No specific labeling was identified in these controls. For double- and triple-immunofluorescence labeling, sections were sequentially processed with each primary antibody and detected with appropriate Alexa Fluor-conjugated secondary antibodies or streptavidin as described above.

SDS-PAGE and Immunoblotting

The lumbar spinal cord was quickly removed after decapitation under deep anesthesia with diethyl ether. Each spinal cord tissue was homogenized in a lysis buffer containing 10 mM Tris-HCl, pH 7.4, 100 mM NaCl, 500 mM EDTA, and a protease inhibitor cocktail (Complete; Roche Diagnostics, Mannheim, Germany) for 30 sec at 4°C. The lysate was centrifuged at 15,000 rpm for 15 min (4°C), and the supernatant was collected and assayed for protein concentration using a Bradford assay kit (Bio-Rad Laboratories, Hercules, CA). After digestion with protease-free chondroitinase ABC (0.5 U/ml; Seikagaku, Tokyo, Japan) for 3 hr at 37°C, the protein samples were diluted with an equal amount of loading buffer [125 mM Tris-HCl, 5% wt/vol sodium dodecyl sulfate (SDS), pH 6.8], then denatured at 70°C for 5 min. SDS-polyacrylamide gel electrophoresis (SDS-PAGE) was performed in 5–10% gradient gel (Bio-Rad) for neurocan or 5–20% gradient gel (Atto, Tokyo, Japan) for phosphacan, versican, α-tubulin, and β-actin. Lysate equivalent to 3.75 μg protein sample was run on the gel for 180 min for neurocan, 450 min for versican, and 300 min for phosphacan at 100 V, together with size markers (WIDE-VIEW Western size marker; Wako Pure Chemical; Chemiluminescent-BlueRanger Prestained Molecular Weight Marker Mix; Thermo Fisher Scientific, Rockford, IL). Protein samples were then transferred to polyvinylidene difluoride (PVDF) membranes (Immobilon-P; Millipore, Bedford, MA). The membranes were blocked with 6% skim milk in TBS-T (TBS with 0.05% Tween-20) for neurocan and phosphacan or 4% skim milk in TBS-T for versican overnight at 4°C, then incubated with a primary antibody for 1 hr at RT. The primary antibodies employed for immunoblotting were as follows: mouse anti-neurocan monoclonal IgG (1:2,000; Chemicon International); rabbit anti-GAGα domain of versican V2 polyclonal IgG (1:500; Chemicon International), mouse anti-phosphacan/RPTPβ core protein monoclonal IgM, which recognizes secreted phosphacan fragments and full-length phosphacan/RPTPβ (1:1,000; Chemicon International); mouse anti-α-tubulin monoclonal IgG (1:2,000; Sigma-Aldrich, St. Louis, MO); and mouse anti-β-actin monoclonal IgG (1:2,000; Abcam, Cambridge, United Kingdom). After three washes in TBS-T, the membranes were incubated with the appropriate horseradish peroxidase (HRP)-conjugated secondary antibody for 1 hr at RT as follows: goat anti-mouse IgG + IgM (H + L; 1:1,000; Kirkegaard and Perry Laboratories, Gaithersburg, MD), and donkey anti-rabbit IgG (1:1,000; GE Healthcare U.K.). We detected the specific bindings using an ECL Plus kit (GE Healthcare) and luminescent image analyzer (LAS-3000 mini; Fuji Photo Film, Tokyo, Japan). To ascertain specific binding of the antibody for each protein, another membrane was stained in a similar way without the primary antibody. The protein expression levels of interest were normalized to those of α-tubulin or β-actin.

Image Analysis and Quantification

We analyzed six to eight transverse sections from each lumbar spinal cord by individual immunofluorescence (n = 3–4, for each experimental group). The selected sections were separated by at least 50 μm from each other. At ×200 magnification under a confocal laser scanning microscope (CLSM) system equipped with HeNe-green (543 nm), HeNe-red (633 nm), and Ar (488 nm) laser units (FV300; Olympus Optical, Tokyo, Japan), we captured images of the defined areas (1,024 × 1,024 pixels for 352 μm × 352 μm) in the ventral horn (VH) and the ventral funiculus (VF) bilaterally, with acquisition software (Fluoview version 4.3; Olympus). The VH image was routinely obtained from the ventrolateral portion of each ventral horn, which covers Rexed's lamina IX at a maximum. The VF image was routinely obtained from the ventral superficial area of white matter in close proximity to the VH. In addition, we captured equal-sized images of the dorsal horns (Rexed's laminae III and VI) and the dorsal funiculi (between the gracile and cuneate fasciculi) for comparative analysis. On double immunofluorescence, images were captured by sequential wavelength excitation and separate detection for each wavelength in order to avoid cross-talk. The collected images were pseudocolored and merged with Fluoview (Olympus). All images of each antibody were collected at identical settings for confocal aperture, laser strength, scan velocity, photomultiplier tube sensitivity, gain, and offset. The images were digitally stored on a PC (ThinkPad; IBM Japan, Tokyo, Japan) as TIFF files with 4,095 shades of gray. We evaluated the immunoreactive area (pixels) in each defined area using computerized software (ImageJ 1.35s; Wayne Rasa, NIH). The thresholds for positive were set at constant (1,590 on 0–4,095 gray scale), and the number of

pixels above the threshold was calculated to express the CSPG-immunoreactive area. To assess the histological progression of MND phenotype, we evaluated the ubiquitin-immunoreactive area in the same way. We also estimated the number of VH neurons in the lumbar spinal cord (L5). In the captured VH images, as described above, Hu C/D-immunoreactive neurons (Liu et al., 1995) with distinct nuclei and a diameter greater than 25 μm (Gadomski et al., 2006) were counted in a fixed area (470 μm × 470 μm) using ImageJ (NIH). The average number of bilateral VH images from eight sections separated at least 50 μm from each other was submitted for statistical analysis in individual animals. For quantification of immunoblotting, the average optical densities (expressed in arbitrary units) for the specific bands were measured in ImageJ (NIH). The area showing negative immunoreaction was treated as background density. The value was normalized with the average optical densities of the immunoreactive band for α-tubulin or β-actin in each lane individually.

Statistical Analysis

All the results are expressed as mean ± SD. Differences among the rat groups were examined for significance using one-way ANOVA among means of value, with the category of rats as the independent factor. Multiple pairwise comparisons between means were tested by the Tukey-Kramer post hoc test when ANOVA showed significant differences ($P < 0.05$). For quantification of immunoblotting, differences between the two groups were evaluated by means of Student's *t*-test for paired data. All statistical analysis was performed with PC software (GraphPad Prism 5; GraphPad Software, San Diego, CA), and the null hypothesis was rejected at the 0.05 level.

RESULTS

Neuropathology in Tg Rats

To evaluate the histopathological hallmarks such as neuronal loss and abnormal protein aggregates (Watanabe et al., 2001; for review see Kabashi and Durham, 2006), we performed triple immunofluorescence for Hu C/D, pNF, and Ub in lumbar spinal cord at three different stages. The number of large ventral horn neurons we examined was immunoreactive for Hu C/D (Liu et al., 1995), with the distinct nuclei and a diameter greater than 25 μm. Therefore, the estimated number was essentially interpreted as the number of motor neurons in rat spinal cord (Gadomski et al., 2006). For the sections of non-Tg rats, we observed no significant neuronal loss or significant pNF- and Ub-immunoreactive aggregates in the ventral horns (Fig. 1Aa–c,B,C). At the Pre stage, there was no significant difference in the number of large VH neurons between Tg rats and the age-matched Non-Tg littermates (Fig. 1Aa,d,B). From the ES stage, however, the number of large VH neurons in Tg rats showed a progressive and significant decrease compared with their age-matched littermates (Fig. 1Ab,c,e,f,B; $P < 0.01$). The progressive loss of neurons was consistent through the disease progression, as was reported previously (Nagai et al., 2001), and was significant between Tg rats at the Pre and ES stages (Fig. 1B; $P < 0.01$), whereas the statistics did not show significant difference in the symptomatic phase (between the ES and LS stages; Fig. 1B). To address the neurodegeneration aside from the neuronal loss in Tg rats, we quantified the emergence of abnormal protein aggregates in the ventral horns. From the ES stages, Tg rats showed a progressive increase of Ub- and/or pNF-immunoreactive dot- or rod-shaped aggregates in the VH neuropil (Fig. 1Ae,f). At the LS stage, we found abnormally pNF-accumulated neuronal cell body (Fig. 1Ag, arrows) with more frequent Ub- and/or pNF-immunoreactive aggregates in the ventral horns of Tg rats (Fig. 1Af,inset,g, arrows). The Ub-positive aggregates were often colocalized with or surrounded by pNF-immunoreactive structures (Fig. 1Ae,f,inset,g), suggesting intraneuronal accumulation of abnormal proteins. Furthermore, statistical analysis of immunolabeling for Ub revealed a significant and progressive increase of Ub-positive structures in Tg rats compared with non-Tg rats at the ES and LS stages (Fig. 1C; $P < 0.01$), and also among Tg rats at the three stages (Pre, ES, and LS; Fig. 1C; $P < 0.01$).

Increased CSPG Immunoreactivity in Tg Rats

To examine a possible accumulation of CSPG in the spinal cord with ALS-like motor neuron degeneration, we employed a series of immunofluorescence using antibodies specific for CSPG core proteins such as neurocan, versican, and phosphacan at different stages. In the spinal cord of non-Tg rats, mild and sparse perineuronal immunoreactivity for neurocan was observed throughout the parenchyma (Fig. 2a,e). The dorsal horns of the gray matter (data not shown) and the subpial zone of the white matter (Fig. 2e) were predominantly immunoreactive for neurocan in non-Tg sections. In contrast, Tg rats showed markedly increased immunoreactivity at all the examined stages compared with age-matched non-Tg littermates (Fig. 2b–d,f–h). Notably, the up-regulation of neurocan immunoreactivity was predominant in the ventral spinal cord (VH and VF; Fig. 2b–d,f–h) in Tg rat and spread over the dorsal spinal cord (not shown) at the symptomatic (ES and LS) stages. In addition, we frequently observed distinct perineuronal immunoreactivity for neurocan in VH of Tg rats (Fig. 2b–d, arrows). Furthermore, quantification of immunolabeling revealed a significant and progressive increase of neurocan immunoreactivity in Tg rats even from Pre stage compared with non-Tg rats. Among Tg rats, there was a significant increase of neurocan immunoreactivity in both ES and LS stages compared with Pre stage (Fig. 3).

As for versican, we detected a constitutive expression at low levels in both the gray and the white matter in non-Tg spinal cord (Fig. 2i,m). In Tg rats, versican immunoreactivity was also up-regulated in the ventral spinal cord (VH and VF) even at the Pre stage (Fig. 2j–l,n–p). Quantification of immunolabeling showed a significant increase of versican immunoreactivity in the ventral spinal cord of Tg rats compared with non-Tg rats (Fig. 3).

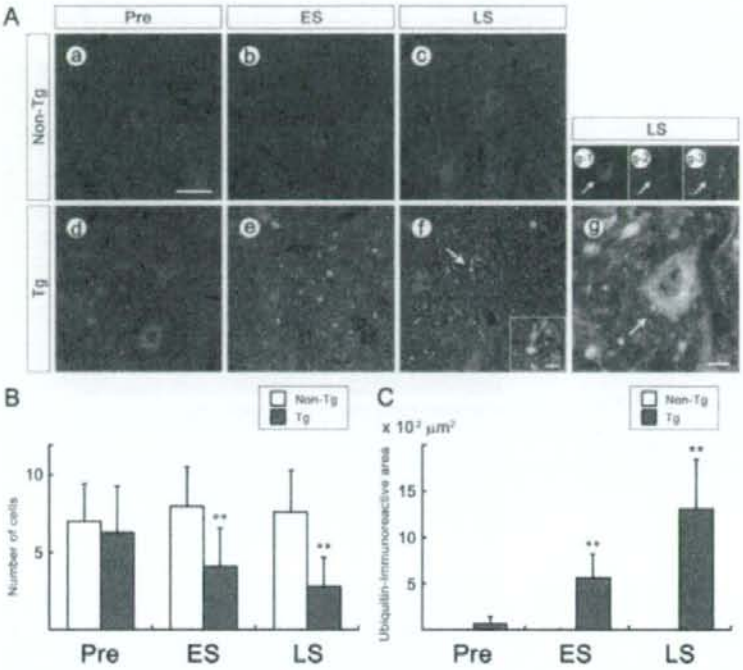

Fig. 1. Progressive pathology of spinal ventral horns in H46R transgenic (Tg) rats. **A:** Representative microphotographs of triple immunofluorescence for ubiquitin (Ub, green), phosphorylated neurofilament-M and -H (pNF, red), and neuronal protein Hu C/D (blue) in ventral horns of lumbar spinal cord. Red and blue color colocalization shows as magenta, green and blue colocalization shows as cyan, green and red colocalization shows as yellow, and colocalization of all three shows as white. Tg rats at presymptomatic (Pre) stage (d), early symptomatic (ES) stage (e), and late symptomatic (LS) stage (f) are depicted with those of age-matched littermate controls (non-Tg; a: 24 weeks, b: 26 weeks, c: 28 weeks of age). Ub-positive deposits were observed progressively from the ES stage (e) to the LS stage (f). The deposits (green) were often colocalized with or surrounded by phosphorylated neurofilament-positive structures (red) in Tg rats [e,f(arrow and inset),g]. An abnormally pNF-accumulated neuronal cell body was occasionally found in Tg rats (g). Hu C/D-positive neuron (blue, g-1), pNF-positive soma (red, g-2), Ub-positive deposits (green, g-3); g is an overlay of g-1–3). Arrows indicate a representative large ventral horn neuron that contains Ub-positive deposits with abnormally pNF-accumulated soma (g and g1–3). Transverse sections are oriented so that dorsal is upward. **B:** A significant and progressive decrease in the number of ventral horn neurons in Tg rats at the symptomatic stage (ES and LS). The Hu C/D-immunoreactive neurons (>25 μm in diameter) were counted electronically with ImageJ. The progressive loss of neurons was consistent through the disease progression, and was significant between Tg rats at the Pre and ES stages. **C:** Semiquantification of the Ub immunoreactivity revealed a significant and progressive increase in ubiquitin-positive deposits in the ventral horns. Open bars show the data of age-matched non-Tg littermates, whereas solid bars show those of Tg rats (means ± SD, n = 3 per experimental group, one-way ANOVA followed by the Tukey-Kramer post hoc test). Asterisks indicate a significant difference between Tg and the age-matched non-Tg rats at each stage (**$P < 0.01$). Scale bars = 50 μm in f (applies to a–f); 10 μm in inset; 10 μm in g.

In contrast to neurocan, the up-regulation of versican peaked at the ES stage and diminished at the LS stage in VH of Tg rats. Among Tg rats, versican immunoreactivity in the VH was significantly higher at the ES stage compared with the Pre stage (Fig. 3). However, the versican as well as neurocan immunoreactivity in the VF showed a progressive increase in Tg rats (Fig. 3). Among Tg rats, the immunoreactivity in the VF was significantly higher at the ES and LS stage compared with the Pre stage (Fig. 3). In the dorsal horn of Tg rats as well as in the VH, the immunoreactivity for versican was significantly increased but less prominent than that in the ventral horns at the ES and LS stage (data not shown). On the other hand, there was no significant difference in versican immunolabeling of the dorsal funiculi among Tg rats at the three stages (data not shown).

For phosphacan immunofluorescence, we detected low levels of immunoreactivity in non-Tg spinal cord (Fig. 4i,m). As well as neurocan, phosphacan immunoreactivity in non-Tg was predominant in perineuronal structures in the gray matter and subpial/outer zone of the white matter (Fig. 4i,m). In contrast, Tg rats showed up-regulation of phosphacan at the symptomatic (ES and LS) stages (Fig. 4j,n). Quantification of phosphacan

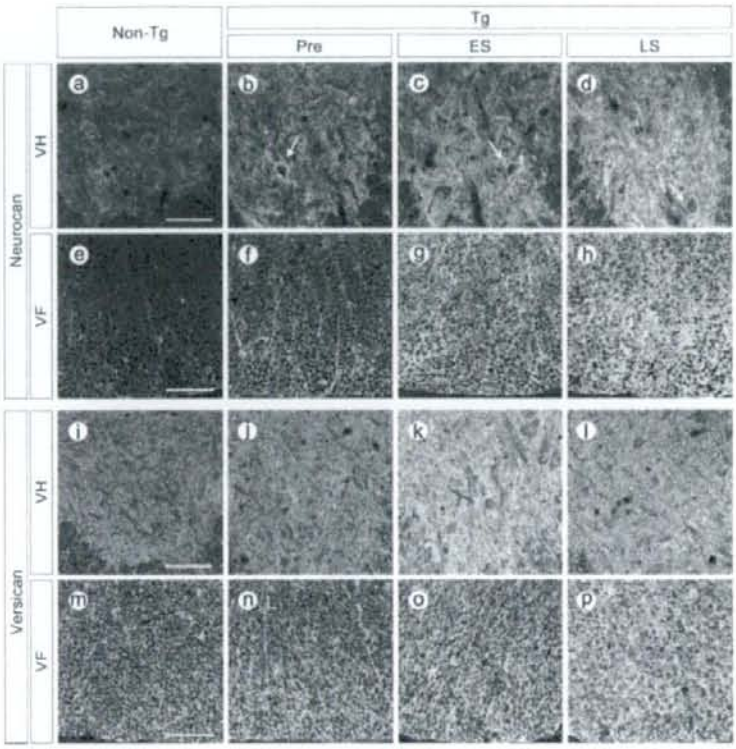

Fig. 2. Representative microphotographs of immunofluorescence for neurocan (a–h, upper panels) and versican (i–p, lower panels) in the ventral spinal cord. In H46R transgenic (Tg) rats, progressive increase of neurocan and versican immunoreactivity was observed in the ventral horns (VH; b–d,j–l) and in the ventral funiculi (VF; f–h,n–p), whereas such an increase was not observed in non-Tg rats (VH; a,i; VF; e,m). Pre, presymptomatic stage (b,f,j,n); ES, early symptomatic stage (c,g,k,o); LS, late symptomatic stage (d,h,l,p); and non-Tg, age-matched littermates corresponding to the ES stage (a,e,i,m). Arrows indicate dense neurocan immunoreactivities around neurons (b–d). Transverse sections are oriented so that dorsal is upward. Scale bars = 100 μm.

immunolabeling in VF revealed a progressive and significant increase in Tg rats at both the ES and the LS stages compared with non-Tg rats (Fig. 3). Among Tg rats, there was a significant increase of phosphacan immunoreactivity in both ES and LS stages compared with Pre stage (Fig. 3). In VH, however, we found a significant increase in Tg rats only at the ES stage (Fig. 3). At the LS stage, phosphacan immunoreactivity in VH of Tg rats returned to the normal level and was not significantly different compared with non-Tg (Fig. 3). There was no significant difference in phosphacan immunoreactivity in the dorsal horns and dorsal funiculi between Tg and Non-Tg rats at any stage (data not shown).

Association Between CSPGs and GFAP-Positive Astrocytes in Tg Rats

GFAP-positive reactive astrocytes increased even at the Pre stage, preceding loss of VH neurons in Tg rats (data not shown). As the disease progressed, the GFAP immunoreactivity became prominent continually not only in the VH but also in the white matter surrounding the VH, especially in the ventral side of spinal cord in Tg rats (Fig. 4c,g,k,o). In a similar way, Iba-1-positive microglia increased progressively in the spinal cord of Tg rats from the Pre stage (data not shown). At the LS stage, we observed numerous hypertrophic reactive astrocytes and reactive microglia predominantly in the ventral spinal cord gray and white matter.

To clarify the cellular source of accumulated CSPGs in the spinal cord, we performed double immunofluorescence for the series of CSPG core proteins with cell type-selective markers as follows: GFAP, an astrocyte marker (Pegram et al., 1985); GST-π, mature oligodendrocytes (Tansey and Cammer, 1991; Tamura et al., 2007); neurofilament-H, large-diameter myelinated neurons (Perry and Lawson, 1993); and Iba-1, resting and activated microglia (Ito et al., 1998; Ahmed et al., 2007). The combinatorial immunolabelings revealed a partial colocalization between neurocan/phosphacan and GFAP (Fig. 4c,d,g,h for neurocan/GFAP; Fig. 4k,l,o,p for phosphacan/GFAP). Colocalization was observed predominantly in the ventral spinal cord (VH and VF), especially in the perineuronal areas immunoreactive for CSPGs in VH (Fig. 4d,l). In contrast, we did not observe any distinct colocalization between CSPGs and other cellular markers such as GST-π, neurofilament-H, and Iba-1 (data not shown).

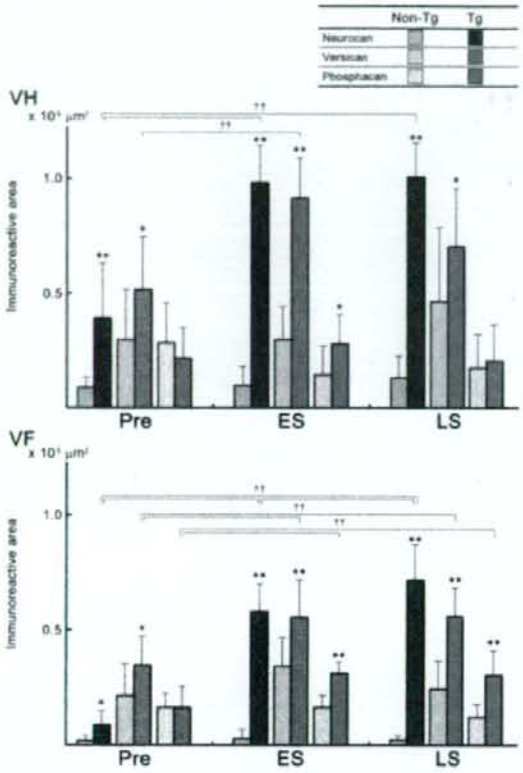

Fig. 3. Semiquantification of the immunofluorescence for different chondroitin sulfate proteoglycan core proteins in the ventral spinal cords of H46R transgenic (Tg) rats and age-matched littermate controls (non-Tg). The immunoreactive areas for various CSPG core proteins are shown by color legends in the figure. The immunoreactive areas of neurocan, versican, and phosphacan were increased in the ventral horns (VH; upper graph) and ventral funiculi (VF; lower graph) in Tg rats but not in Non-Tg rats in each stage (means ± SD, n = 3–4, one-way ANOVA followed by the Tukey-Kramer post hoc test). Asterisks indicate a significant difference between Tg and the age-matched non-Tg rats at each stage ($*P < 0.05$, $**P < 0.01$). Daggers indicate a significant difference in Tg rats between the stages ($††P < 0.01$).

Increased Levels of CSPGs in Tg Rats

To confirm the results of immunohistochemical analysis, we examined the cumulative species of CSPGs in Tg rats by quantitative immunoblotting with specific antibodies for the core proteins. According to the immunofluorescence data (Fig. 3), we selected the examined stages for the CSPG immunoblotting: LS stage for neurocan and ES stage for both versican and phosphacan. The immunoblotting revealed increased levels of distinct CSPG species in whole lumbar spinal cord lysate of Tg rats. For neurocan, immunoblotting showed the increased levels of two isoforms of neurocan in the spinal cord of Tg rats at the LS stage. In non-Tg rats, only thin bands for the proteolytic fragments of neurocan were detected at approximately 150 kDa, without specific bands for the full-length neurocan (Fig. 5A). In contrast, we detected distinct bands specific for both the full length at 245 kDa and for the proteolytic fragments at approximately 150 kDa in Tg rats (Fig. 5A). Densitometry revealed an approximately 40-fold increase of full-length neurocan and fourfold increase of proteolytic fragments of neurocan in the spinal cord of Tg rats compared with those of non-Tg rats (Fig. 5A). As for versican, we found the increased levels of the CNS-specific V2 isoform in the spinal cord of Tg rats at the ES stage. A distinct band corresponding to versican V2 at >220 kDa was evident in Tg rats, whereas very thin bands at the same molecular weight in non-Tg rats (Fig. 5B). Densitometry revealed an approximately fourfold increase of versican V2 in the spinal cord of Tg rats compared with those of non-Tg rats at the ES stage (Fig. 5B). We also found a similar result in the quantitative immunoblotting for phosphacan at the ES stage. The immunoblotting showed a smear-like band corresponding to phosphacan/RPTPβ core protein at >220 kDa. Other bands corresponding to splice variants of phosphacan were also detected at approximately 180 kDa (Fig. 5C). Densitometry revealed an approximately threefold increase of phosphacan/RPTPβ in the spinal cord of Tg rats compared with those of non-Tg rats at the ES stage. Although a similar tendency was observed in the splice variants of phosphacan, there was no significant difference between Tg rats and non-Tg rats at the stage (Fig. 5C). In contrast to the case for the ES stage, we found no significant increase in the levels of versican and phosphacan in Tg rats at the LS stage (data not shown).

DISCUSSION

In the present study, we found a significant accumulation of CSPGs in the adult spinal cord of a rat ALS model. The accumulation was predominant in the ventral spinal cord, where the neuropathology primarily occurred, and subsequently spread throughout the dorsal spinal cord. Moreover, in parallel with disease progression even from the Pre stage, we detected an accelerated increase in both neurocan and versican immunoreactivity. Therefore, it is suggested that the up-regulation of CSPGs is closely related to the neurodegeneration in the present model. However, up-regulation of phosphacan was less prominent as well as less significant only in the ES stage in the ventral horns. Previous studies have reported diverse results for phosphacan after various forms of CNS injury (McKeon et al., 1999; Moon et al., 2002; Tang et al., 2003) or demyelinating lesions (Sobel and Ahmed, 2001). Thus, the differential accumulation of CSPGs suggests a distinct property of each CSPG and a complicated regulation of CSPG metabolism under disease conditions (Galtrey and Fawcett, 2007).

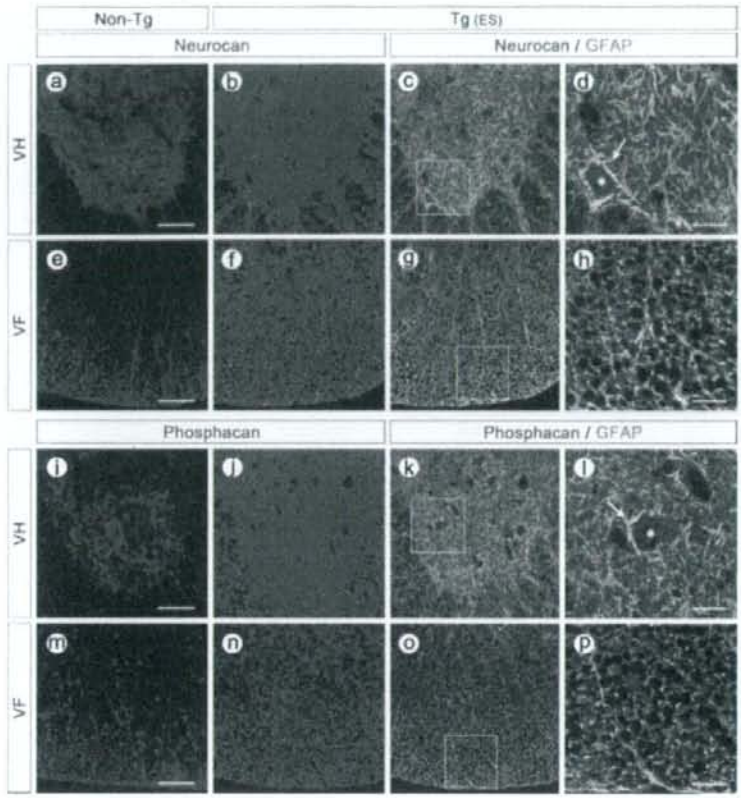

Fig. 4. Representative microphotographs of double immunofluorescence for neurocan (upper panels) or phosphacan (lower panels) with glial fibrillary acidic protein (GFAP). As shown in Figures 2 and 3, the immunofluorescence revealed up-regulation of the CSPG core proteins in the ventral horns (VH) and ventral funiculi (VF) in the spinal cord of H46R transgenic (Tg) rats at the early symptomatic (ES) stage (b,f for neurocan; j,n for phosphacan) but not in the age-matched littermate controls (non-Tg; a,e for neurocan; i,m for phosphacan). Moreover, partial colocalization of neurocan (green in c,d,g,h) or phosphacan (green in k,l,o,p) with GFAP (magenta in the same panels) was detected under confocal laser scanning microscopy in both VH and VF. Especially in VF, close colocalization was observed between neurocan/phosphacan and GFAP immunoreactivities (g,h,o,p). Images were pseudocolored and merged. Magnified view of c, g, k, and o are shown in panels d, h, l, and p, respectively. Asterisks indicate neurons that were surrounded by neurocan or phosphacan immunoreactivities; arrows indicate intense colocalization between neurocan/phosphacan and GFAP immunoreactivities around neurons (d,l). Transverse sections are oriented so that dorsal is upward. Scale bars = 100 μm in a–c,e–g,i–k,m–o; 30 μm in d,h,l,p.

CSPGs are heterogeneous, and each has its own core protein. Each core protein has a different degree of chondroitin sulfate glycosaminoglycan (GAG) chains. Neurocan, as well as versican V2 (which contains only the GAGα domain), phosphacan, and brevican, is expressed specifically in the adult CNS and constitutes a major component of the ECM. During development, CSPGs regulate axonal pathfinding, synaptogenesis, and cell migration and restrict plasticity. Furthermore, CSPGs are reported to bind and interact with a variety of molecules such as growth factors, cytokines, and cell-surface receptors. In gray matter of adult rat spinal cord, CSPGs are distributed mainly in the neuropil, and the VH neurons are surrounded by distinct ECM containing CSPGs, which is called *perineuronal nets* (Vitellaro-Zuccarello et al., 2007). Our findings of immunofluorescence for CSPGs in non-Tg rats are fundamentally compatible with the previous report. Therefore, CSPGs play a physiologically pivotal role such as signal transmission in the intact adult spinal cord and are believed to prevent unnecessary synaptic connections for stabilizing the CNS structure.

Extensive investigations have previously revealed up-regulation of CSPGs in acute insults of CNS. In

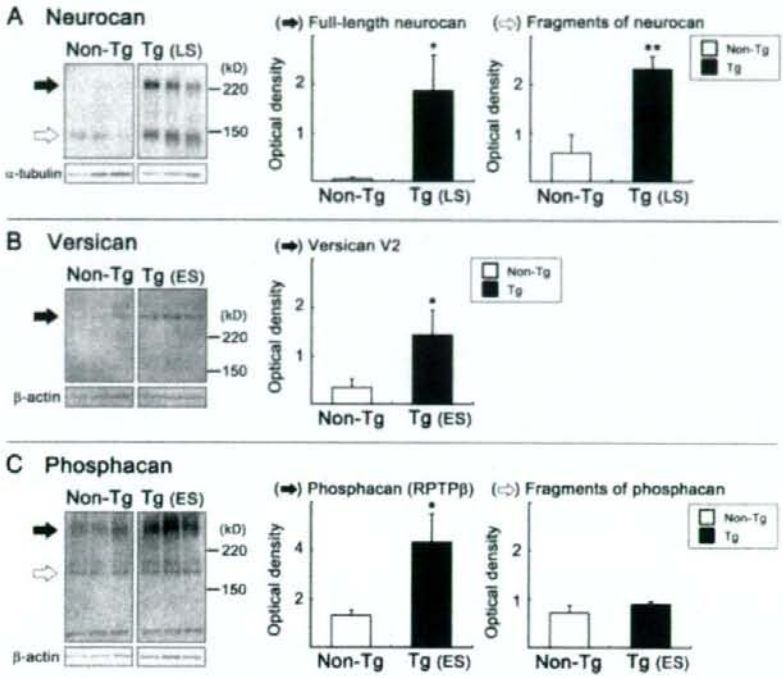

Fig. 5. Quantitative immunoblotting analysis of different chondroitin sulfate proteoglycan (CSPG) levels in the whole lumbar spinal cord of H46R transgenic (Tg) rats and the age-matched littermate controls (non-Tg). Graphs represent relative optical density value of the bands: ratios of those of CSPG to those of the internal control protein are shown (mean ± SD). Asterisks indicate a significant difference between Tg rats and non-Tg rats ($*P < 0.05$, $**P < 0.01$; n = 3, Student's *t*-test). **A:** Immunoblotting for neurocan in Tg rats at the late symptomatic (LS) stage and non-Tg controls. The level of both isoforms of neurocan: the 245-kDa full-length neurocan (solid arrow) and the cleavage products (open arrow) were up-regulated (upper panel). α-Tubulin was used as an internal control for applied amounts of protein in each lane (lower panel). **B:** Immunoblotting for CNS-specific isoform of versican V2 in Tg rats at the early symptomatic (ES) stage and non-Tg controls. The level of versican V2 isoform (>220 kDa, solid arrow) was up-regulated (upper panel). β-Actin was used as a control (lower panel). **C:** Immunoblotting for phosphacan in Tg rats at the ES stage and non-Tg controls. The level of both phosphacan/RPTPβ core protein (>220 kDa, solid arrow) and the fragments (open arrow) were up-regulated (upper panel). β-Actin was used as a control (lower panel).

most cases of acute CNS insults, including cerebrocortical wound injury (McKeon et al., 1991), ischemia (Deguchi et al., 2005), demyelinating lesions (Sobel and Ahmed, 2001), kainic acid-induced excitotoxic lesions (Matsui et al., 2002; Okamoto et al., 2003), and spinal cord injury (Jones et al., 2002; Tang et al., 2003), high levels in the expression of CSPGs peak after a certain period and recover to the normal levels. We found a similar up-regulation of CSPGs even under conditions of a chronic neurodegenerative disease. However, progressive accumulation of neurocan in concert with relentless neuronal loss showed a temporal profile distinct from that of acute CNS injury. Much evidence suggests that CSPGs have inhibitory potentials on axonal regeneration in vitro and in vivo (Galtrey and Fawcett, 2007). Furthermore, more recent studies have shown that the gliosis-associated CSPGs play an additional inhibitory role in cell migration in vivo (Kearns et al., 2003; Ikegami et al., 2005). Thus, the accumulation of CSPGs could inhibit endogenous/exogenous regenerative potential as a molecular barrier. The inhibitory property of CSPGs is derived from both the GAG side chains and the core proteins themselves. Thus, the suppression of CSPG expression or enzymatic degradation of CSPGs may change the microenvironment of spinal cord in the present model. In fact, local digestion of GAG side chains in vivo by chondroitinase ABC, a bacteria-derived enzyme, has previously been shown to induce axonal elongation and promote functional recovery in spinal cord injury models (Moon et al., 2001; Bradbury et al., 2002) and also to create a permissive environment conducive to axonal growth from peripheral nerve graft into spinal cord (Houle et al., 2006).

On the other hand, a neuroprotective role of CSPGs has also been suggested in several CNS insults, such as spinal cord injury, excitotoxicity, and β-amy-

loid-induced neurodegeneration models (Rhodes and Fawcett, 2004). Considering the possible beneficial aspects of CSPGs, the up-regulation of CSPGs surrounding residual VH neurons may reflect an endogenous protective process against the neurodegeneration in the present model. Although enzymatic digestion of CSPGs has not been reported to exacerbate CNS damage to date (Galtrey and Fawcett, 2007), the significance of the abnormally accumulated CSPGs in various types of CNS insults is still a matter of debate. Reactive gliosis, one of the prominent pathological events in ALS spinal cord (Neusch et al., 2007), consists mainly of reactive astrocytes (Silver and Miller, 2004). In addition to the astrocytic reaction, microglial activation is also an early and distinct response in Tg rodent models of ALS (Hall et al., 1998; Alexianu et al., 2001). In the present study, double immunofluorescence revealed partial associations between neurocan/phosphacan and GFAP-positive astrocytes, but not Iba-1-positive microglia, in the degenerating spinal cord of Tg rats. Hypertrophic astrocytes are principal source of neurocan and secrete it into the ECM in adult CNS. In addition, neurons are reported to synthesize neurocan. Astrocytes have also been reported to produce phosphacan following brain injury (McKeon et al., 1999; Thon et al., 2000). Consistently with these data, we observed the perineuronal dense staining around VH neurons, where GFAP-positive processes surround the neuronal cell body, in the spinal cord of Tg rats. More systematic investigation to identify the cellular source of CSPGs using this model is necessary. Because reactive astrocytes are considered to play paradoxical roles both beneficial and harmful to neurons (Sofroniew, 2005), identification of the mechanisms that regulate the molecules in the ECM could lead to control of the expression of CSPGs. In fact, a recent study demonstrated the CSPG-regulating molecules in astrocytes. Xylosyltransferase and chondroitin 4-sulfotransferase are responsible for chondroitin sulfate side chain synthesis by astrocytes (Gris et al., 2007). Transforming growth factor-β2, interleukin-6, and platelet-derived growth factor are also reported to regulate differentially the expression of CSPGs in astrocytes (Gris et al., 2007). In addition, proteases involved in the turnover of CSPG core proteins are reported, such as the matrix metalloproteinases (MMPs) and a disintegrin and metalloproteinase with thrombospondin repeats (ADAMTSs). MMPs are rapidly up-regulated after almost all types of CNS insult, including spinal cord injury (de Castro et al., 2000), ischemia (Rosenberg, 1995; Muir et al., 2002), and Alzheimer's disease (Yoshiyama et al., 2000). Further study will be needed to elucidate the possible roles of these regulatory molecules in CSPG metabolism in vivo.

Neurocan is one of the major CSPGs in the intact CNS. During development, expression of both the full-length (245 kDa) neurocan and its cleaved fragments, C-terminal (150 kDa) and N-terminal (130 kDa) neurocan, is regulated in the normal brain (Rauch et al., 1991; Meyer-Puttlitz et al., 1995). In the intact adult CNS, full-length neurocan is scarcely detected, whereas the N-terminal fragment has been detected throughout life (Matsui et al., 1994). Moreover, both full-length and N-terminal neurocan, but not C-terminal fragments, show an inhibitory activity against neurite outgrowth (Katoh-Semba et al., 1998; Asher et al., 2000). Thus, it is suggested that full-length neurocan plays the most important role among its isoforms in regulating neural plasticity. Immunoblotting analysis in the present study showed a robust increase of the full-length neurocan and its fragments at the LS stage, further suggesting an inhibitory microenvironment for regeneration in this model. Similar changes have been reported in excitotoxic epileptic conditions (Matsui et al., 2002) and after mechanical incision, ischemia (Deguchi et al., 2005), and spinal cord injury (Tang et al., 2003). In contrast to those of neurocan, functional properties of versican, phosphacan, and their isoforms under physiological or pathological conditions remains to be established. Among three alternatively spliced variants, versican V2 is abundant in the adult CNS and is expressed by oligodendrocyte-lineage cells, whereas V1 isoform is distributed widely around the other tissue. Among the isoforms, versican V2 is considered to be inhibitory to neurite outgrowth, but how the isoforms of versican are controlled after CNS insults is unclear (Viapiano and Matthews, 2006). On the other hand, phosphacan is an extracellular part of the RPTPβ receptor, and the phosphacan/RPTPβ has at least four spliced variants. In addition to the presence of various isoforms of phosphacan/RPTPβ, their functional roles have been shown to be highly complicated. Previous reports showed diverse function (promotion or inhibition) on axonal regrowth, which depends on the mode of expression and molecules with which to interact (Faissner et al., 2006). As well as neurocan, both neurons and reactive astrocytes are reported to express phosphacan/RPTPβ. The significance of increased phosphacan in this study remains to be defined.

In summary, this is the first study to show the spatiotemporal accumulation of CSPGs under chronic neurodegenerative condition in a Tg rat model of ALS. Although the possible neuroprotective implication remains to be investigated, the increased CSPGs and their association with reactive astrocytes suggest the existence of a non-permissive microenvironment for regeneration. Considering the future development of cell-restorative therapy in ALS, both the regulation of the microenvironment surrounding motor neurons and the control of reactive gliosis may be an important strategy in facilitating survival, migration, neurite outgrowth, and synaptogenesis of newborn cells.

ACKNOWLEDGMENTS

We sincerely thank N. Agatsuma and T. Kibushi for technical assistance.

REFERENCES

Ahmed Z, Shaw G, Sharma VP, Yang C, McGowan E, Dickson DW. 2007. Actin-binding proteins coronin-1a and IBA-1 are effective

microglial markers for immunohistochemistry. J Histochem Cytochem 55:687–700.

Alexianu ME, Kozovska M, Appel SH. 2001. Immune reactivity in a mouse model of familial ALS correlates with disease progression. Neurology 57:1282–1289.

Aoki M, Ogasawara M, Matsubara Y, Narisawa K, Nakamura S, Itoyama Y, Abe K. 1993. Mild ALS in Japan associated with novel SOD mutation. Nat Genet 5:323–324.

Asher RA, Morgenstern DA, Fidler PS, Adcock KH, Oohira A, Braistead JE, Levine JM, Margolis RU, Rogers JH, Fawcett JW. 2000. Neurocan is upregulated in injured brain and in cytokine-treated astrocytes. J Neurosci 20:2427–2438.

Boillee S, Vande Velde C, Cleveland DW. 2006a. ALS: a disease of motor neurons and their nonneuronal neighbors. Neuron 52:39–59.

Boillee S, Yamanaka K, Lobsiger CS, Copeland NG, Jenkins NA, Kassiotis G, Kollias G, Cleveland DW. 2006b. Onset and progression in inherited ALS determined by motor neurons and microglia. Science 312:1389–1392.

Bradbury EJ, Moon LD, Popat RJ, King VR, Bennett GS, Patel PN, Fawcett JW, McMahon SB. 2002. Chondroitinase ABC promotes functional recovery after spinal cord injury. Nature 416:636–640.

Busch SA, Silver J. 2007. The role of extracellular matrix in CNS regeneration. Curr Opin Neurobiol 17:120–127.

Chi L, Ke Y, Luo C, Li B, Gozal D, Kalyanaraman B, Liu R. 2006. Motor neuron degeneration promotes neural progenitor cell proliferation, migration, and neurogenesis in the spinal cords of amyotrophic lateral sclerosis mice. Stem Cells 24:34–43.

Clement AM, Nguyen MD, Roberts EA, Garcia ML, Boillee S, Rule M, McMahon AP, Doucette W, Siwek D, Ferrante RJ, Brown RH Jr, Julien JP, Goldstein LS, Cleveland DW. 2003. Wild-type nonneuronal cells extend survival of SOD1 mutant motor neurons in ALS mice. Science 302:113–117.

de Castro RC Jr, Burns CL, McAdoo DJ, Romanic AM. 2000. Metalloproteinase increases in the injured rat spinal cord. Neuroreport 11: 3551–3554.

Deguchi K, Takashi M, Hayashi T, Oohira A, Nagotani S, Li F, Jin G, Nagano I, Shoji M, Miyazaki M, Abe K, Huh NH. 2005. Expression of neurocan after transient middle cerebral artery occlusion in adult rat brain. Brain Res 1037:194–199.

DeWitt DA, Silver J, Canning DR, Perry G. 1993. Chondroitin sulfate proteoglycans are associated with the lesions of Alzheimer's disease. Exp Neurol 121:149–152.

DeWitt DA, Richey PL, Praprotnik D, Silver J, Perry G. 1994. Chondroitin sulfate proteoglycans are a common component of neuronal inclusions and astrocytic reaction in neurodegenerative diseases. Brain Res 656:205–209.

Faissner A, Heck N, Dobbertin A, Garwood J. 2006. DSD-1-proteoglycan/phosphacan and receptor protein tyrosine phosphatase-beta isoforms during development and regeneration of neural tissues. Adv Exp Med Biol 557:25–53.

Gadomski R, Chrapusta SJ, Wojda R, Grieb P. 2006. Morphological changes and selective loss of motoneurons in the lumbar part of the spinal cord in a rat model of familial amyotrophic lateral sclerosis (fALS). Fol Neuropathol 44:154–161.

Gage FH. 2000. Mammalian neural stem cells. Science 287:1433–1438.

Galtrey CM, Fawcett JW. 2007. The role of chondroitin sulfate proteoglycans in regeneration and plasticity in the central nervous system. Brain Res Rev 54:1–18.

Gris P, Tighe A, Levin D, Sharma R, Brown A. 2007. Transcriptional regulation of scar gene expression in primary astrocytes. Glia 55:1145–1155.

Guan YJ, Wang X, Wang HY, Kawagishi K, Ryu H, Huo CF, Shimony EM, Kristal BS, Kuhn HG, Friedlander RM. 2007. Increased stem cell proliferation in the spinal cord of adult amyotrophic lateral sclerosis transgenic mice. J Neurochem 102:1125–1138.

Gurney ME, Pu H, Chiu AY, Dal Canto MC, Polchow CY, Alexander DD, Caliendo J, Hentati A, Kwon YW, Deng HX, et al. 1994. Motor neuron degeneration in mice that express a human Cu, Zn superoxide dismutase mutation. Science 264:1772–1775.

Hall ED, Oostveen JA, Gurney ME. 1998. Relationship of microglial and astrocytic activation to disease onset and progression in a transgenic model of familial ALS. Glia 23:249–256.

Haverkamp LJ, Appel V, Appel SH. 1995. Natural history of amyotrophic lateral sclerosis in a database population. Validation of a scoring system and a model for survival prediction. Brain 118:707–719.

Horner PJ, Power AE, Kempermann G, Kuhn HG, Palmer TD, Winkler J, Thal LJ, Gage FH. 2000. Proliferation and differentiation of progenitor cells throughout the intact adult rat spinal cord. J Neurosci 20: 2218–2228.

Houle JD, Tom VJ, Mayes D, Wagoner G, Phillips N, Silver J. 2006. Combining an autologous peripheral nervous system "bridge" and matrix modification by chondroitinase allows robust, functional regeneration beyond a hemisection lesion of the adult rat spinal cord. J Neurosci 26:7405–7415.

Ikegami T, Nakamura M, Yamane J, Katoh H, Okada S, Iwanami A, Watanabe K, Ishii K, Kato F, Fujita H, Takahashi T, Okano HJ, Toyama Y, Okano H. 2005. Chondroitinase ABC combined with neural stem/progenitor cell transplantation enhances graft cell migration and outgrowth of growth-associated protein-43-positive fibers after rat spinal cord injury. Eur J Neurosci 22:3036–3046.

Ito D, Imai Y, Ohsawa K, Nakajima K, Fukuuchi Y, Kohsaka S. 1998. Microglia-specific localisation of a novel calcium binding protein, Iba1. Brain Res Mol Brain Res 57:1–9.

Jones LL, Yamaguchi Y, Stallcup WB, Tuszynski MH. 2002. NG2 is a major chondroitin sulfate proteoglycan produced after spinal cord injury and is expressed by macrophages and oligodendrocyte progenitors. J Neurosci 22:2792–2803.

Kabashi E, Durham HD. 2006. Failure of protein quality control in amyotrophic lateral sclerosis. Biochim Biophys Acta 1762:1038–1050.

Katoh-Semba R, Matsuda M, Watanabe E, Maeda N, Oohira A. 1998. Two types of brain chondroitin sulfate proteoglycan: their distribution and possible functions in the rat embryo. Neurosci Res 31:273–282.

Kearns SM, Laywell ED, Kukekov VK, Steindler DA. 2003. Extracellular matrix effects on neurosphere cell motility. Exp Neurol 182:240–244.

Liu J, Dalmau J, Szabo A, Rosenfeld M, Huber J, Furneaux H. 1995. Paraneoplastic encephalomyelitis antigens bind to the AU-rich elements of mRNA. Neurology 45:544–550.

Liu Z, Martin LJ. 2006. The adult neural stem and progenitor cell niche is altered in amyotrophic lateral sclerosis mouse brain. J Comp Neurol 497:468–488.

Matsui F, Watanabe E, Oohira A. 1994. Immunological identification of two proteoglycan fragments derived from neurocan, a brain-specific chondroitin sulfate proteoglycan. Neurochem Int 25:425–431.

Matsui F, Kawashima S, Shuo T, Yamauchi S, Tokita Y, Aono S, Keino H, Oohira A. 2002. Transient expression of juvenile-type neurocan by reactive astrocytes in adult rat brains injured by kainate-induced seizures as well as surgical incision. Neuroscience 112:773–781.

Matsumoto A, Okada Y, Nakamichi M, Nakamura M, Toyama Y, Sobue G, Nagai M, Aoki M, Itoyama Y, Okano H. 2006. Disease progression of human SOD1 (G93A) transgenic ALS model rats. J Neurosci Res 83:119–133.

McKeon RJ, Schreiber RC, Rudge JS, Silver J. 1991. Reduction of neurite outgrowth in a model of glial scarring following CNS injury is correlated with the expression of inhibitory molecules on reactive astrocytes. J Neurosci 11:3398–3411.

McKeon RJ, Jurynec MJ, Buck CR. 1999. The chondroitin sulfate proteoglycans neurocan and phosphacan are expressed by reactive astrocytes in the chronic CNS glial scar. J Neurosci 19:10778–10788.

Meyer-Puttlitz B, Milev P, Junker E, Zimmer I, Margolis RU, Margolis RK. 1995. Chondroitin sulfate and chondroitin/keratan sulfate proteoglycans of nervous tissue: developmental changes of neurocan and phosphacan. J Neurochem 65:2327–2337.

Moon LD, Asher RA, Rhodes KE, Fawcett JW. 2001. Regeneration of CNS axons back to their target following treatment of adult rat brain with chondroitinase ABC. Nat Neurosci 4:465–466.

Moon LD, Asher RA, Rhodes KE, Fawcett JW. 2002. Relationship between sprouting axons, proteoglycans and glial cells following unilateral nigrostriatal axotomy in the adult rat. Neuroscience 109:101–117.

Muir EM, Adcock KH, Morgenstern DA, Clayton R, von Stillfried N, Rhodes K, Ellis C, Fawcett JW, Rogers JH. 2002. Matrix metalloproteases and their inhibitors are produced by overlapping populations of activated astrocytes. Brain Res Mol Brain Res 100:103–117.

Nagai M, Aoki M, Miyoshi I, Kato M, Pasinelli P, Kasai N, Brown RH Jr, Itoyama Y. 2001. Rats expressing human cytosolic copper-zinc superoxide dismutase transgenes with amyotrophic lateral sclerosis: associated mutations develop motor neuron disease. J Neurosci 21:9246–9254.

Neusch C, Bahr M, Schneider-Gold C. 2007. Glia cells in amyotrophic lateral sclerosis: new clues to understanding an old disease? Muscle Nerve 35:712–724.

Okamoto M, Sakuyama J, Mori S, Kurazono S, Usui S, Hasegawa M, Oohira A. 2003. Kainic acid-induced convulsions cause prolonged changes in the chondroitin sulfate proteoglycans neurocan and phosphacan in the limbic structures. Exp Neurol 184:179–195.

Pegram CN, Eng LF, Wikstrand CJ, McComb RD, Lee YL, Bigner DD. 1985. Monoclonal antibodies reactive with epitopes restricted to glial fibrillary acidic protein of several species. Neurochem Pathol 3: 119–138.

Perry MJ, Lawson SN. 1993. Neurofilaments in rat and cat spinal cord: a comparative immunocytochemical study of phosphorylated and non-phosphorylated subunits. Cell Tissue Res 272:249–256.

Rauch U, Gao P, Janetzko A, Flaccus A, Hilgenberg L, Tekotte H, Margolis RK, Margolis RU. 1991. Isolation and characterization of developmentally regulated chondroitin sulfate and chondroitin/keratan sulfate proteoglycans of brain identified with monoclonal antibodies. J Biol Chem 266:14785–14801.

Reaume AG, Elliott JL, Hoffman EK, Kowall NW, Ferrante RJ, Siwek DF, Wilcox HM, Flood DG, Beal MF, Brown RH Jr, Scott RW, Snider WD. 1996. Motor neurons in Cu/Zn superoxide dismutase-deficient mice develop normally but exhibit enhanced cell death after axonal injury. Nat Genet 13:43–47.

Rhodes KE, Fawcett JW. 2004. Chondroitin sulphate proteoglycans: preventing plasticity or protecting the CNS? J Anat 204:33–48.

Rosen DR, Siddique T, Patterson D, Figlewicz DA, Sapp P, Hentati A, Donaldson D, Goto J, O'Regan JP, Deng HX, et al. 1993. Mutations in Cu/Zn superoxide dismutase gene are associated with familial amyotrophic lateral sclerosis. Nature 362:59–62.

Rosenberg GA. 1995. Matrix metalloproteinases in brain injury. J Neurotrauma 12:833–842.

Silver J, Miller JH. 2004. Regeneration beyond the glial scar. Nat Rev Neurosci 5:146–156.

Sobel RA, Ahmed AS. 2001. White matter extracellular matrix chondroitin sulfate/dermatan sulfate proteoglycans in multiple sclerosis. J Neuropathol Exp Neurol 60:1198–1207.

Sofroniew MV. 2005. Reactive astrocytes in neural repair and protection. Neuroscientist 11:400–407.

Tamura Y, Kataoka Y, Cui Y, Takamori Y, Watanabe Y, Yamada H. 2007. Intracellular translocation of glutathione S-transferase pi during oligodendrocyte differentiation in adult rat cerebral cortex in vivo. Neuroscience (in press).

Tang X, Davies JE, Davies SJ. 2003. Changes in distribution, cell associations, and protein expression levels of NG2, neurocan, phosphacan, brevican, versican V2, and tenascin-C during acute to chronic maturation of spinal cord scar tissue. J Neurosci Res 71:427–444.

Tansey FA, Cammer W. 1991. A pi form of glutathione-S-transferase is a myelin- and oligodendrocyte-associated enzyme in mouse brain. J Neurochem 57:95–102.

Thon N, Haas CA, Rauch U, Merten T, Fassler R, Frotscher M, Deller T. 2000. The chondroitin sulphate proteoglycan brevican is upregulated by astrocytes after entorhinal cortex lesions in adult rats. Eur J Neurosci 12:2547–2558.

Viapiano MS, Matthews RT. 2006. From barriers to bridges: chondroitin sulfate proteoglycans in neuropathology. Trends Mol Med 12:488–496.

Vitellaro-Zuccarello L, Bosisio P, Mazzetti S, Monti C, De Biasi S. 2007. Differential expression of several molecules of the extracellular matrix in functionally and developmentally distinct regions of rat spinal cord. Cell Tissue Res 327:433–447.

Warita H, Murakami T, Manabe Y, Sato K, Hayashi T, Seki T, Abe K. 2001. Induction of polysialic acid-neural cell adhesion molecule in surviving motoneurons of transgenic amyotrophic lateral sclerosis mice. Neurosci Lett 300:75–78.

Watanabe M, Dykes-Hoberg M, Culotta VC, Price DL, Wong PC, Rothstein JD. 2001. Histological evidence of protein aggregation in mutant SOD1 transgenic mice and in amyotrophic lateral sclerosis neural tissues. Neurobiol Dis 8:933–941.

Yoshiyama Y, Asahina M, Hattori T. 2000. Selective distribution of matrix metalloproteinase-3 (MMP-3) in Alzheimer's disease brain. Acta Neuropathol 99:91–95.

Experimental Neurology 211 (2008) 378–386

Contents lists available at ScienceDirect

Experimental Neurology

journal homepage: www.elsevier.com/locate/yexnr

A dopamine receptor antagonist L-745,870 suppresses microglia activation in spinal cord and mitigates the progression in ALS model mice

Kazunori Tanaka [a,b], Yoshinori Okada [b], Takuya Kanno [a,b,c], Asako Otomo [d], Yoshiko Yanagisawa [a,b,c], Junko Shouguchi-Miyata [a,b], Etsuko Suga [a,b], Eri Kohiki [b], Kyuichiro Onoe [b], Hitoshi Osuga [b], Masashi Aoki [e], Shinji Hadano [c,d], Yasuto Itoyama [e], Joh-E Ikeda [a,c,d,f,*]

[a] NGP Biomedical Research Institute, Neugen Pharma Inc., Tokai University School of Medicine, Isehara, Kanagawa 259-1193, Japan
[b] Department of Molecular Neuroscience, The Institute of Medical Sciences, Tokai University, Isehara, Kanagawa 259-1193, Japan
[c] Department of Molecular Life Sciences, Tokai University School of Medicine, Isehara, Kanagawa 259-1193, Japan
[d] Neurodegenerative Diseases Research Centre, Graduate School of Medicine, Tokai University, Isehara, Kanagawa 259-1193, Japan
[e] Department of Neurology, Tohoku University Graduate School of Medicine, Sendai, Miyagi 980-0872, Japan
[f] Department of Paediatrics, Faculty of Medicine, University of Ottawa, Ontario, Canada K1H 8M5

ARTICLE INFO

Article history:
Received 6 November 2007
Revised 5 February 2008
Accepted 6 February 2008
Available online 4 March 2008

Keywords:
Amyotrophic lateral sclerosis
Cu/Zn superoxide dismutase
Transgenic mice
Oxidative stress
Microglia

ABSTRACT

Amyotrophic lateral sclerosis (ALS) is a neurodegenerative disease characterized by a selective loss of motor neurons in the motor cortex, brainstem, and spinal cord. It has been shown that oxidative stress plays a pivotal role in the progression of this motor neuron loss. We have previously reported that L-745,870, a dopamine D4 receptor antagonist, selectively inhibits oxidative stress-induced cell death *in vitro* and exerts a potent neuroprotective effect against ischemia-induced neural cell damage in gerbil. To investigate the efficacy of L-745,870 in the treatment of ALS, we here conducted a chronic administration of L-745,870 to transgenic mice expressing a mutated form of human superoxide dismutase gene ($SOD1^{H46R}$); a mouse model of familial ALS, and assessed whether the mice benefit from this treatment. The pre-onset administration of L-745,870 significantly delayed the onset of motor deficits, slowed the disease progression, and extended a life span in transgenic mice. These animals showed a delayed loss of anterior horn cells in the spinal cord concomitant with a reduced level of microglial activation at a late symptomatic stage. Further, the post-onset administration of L-745,870 to the $SOD1^{H46R}$ transgenic mice remarkably slowed the disease progression and extended their life spans. Taken together, our findings in a rodent model of ALS may have implication that L-745,870 is a possible novel therapeutic means to the treatment of ALS.

Introduction

Amyotrophic lateral sclerosis (ALS) is a heterogeneous group of inexorable neurodegenerative disorders characterized by a selective loss of upper motor neurons in the motor cortex, and lower motor neurons in the brainstem and spinal cord, culminating in paralysis and death. While the majority of ALS cases are sporadic, 5–10% of patients are familial ALS (fALS) (Cleveland and Rothstein, 2001), among which an approximately 20% are linked to mutations in the gene encoding copper–zinc superoxide dismutase (*SOD1*) (Rosen et al., 1993). Currently, there are a limited number of therapeutic strategies to effectively cure and/or relieve symptoms and improve the quality of life for patients.

Although the mechanisms for the selective degeneration of motor neurons are still unclear, several lines of evidence have indicated that ALS is associated with oxidative stress, excitotoxicity, mitochondrial dysfunction, neurofilament accumulation, neural inflammation, and protein misfolding (Barber et al., 2006; Cluskey and Ramsden, 2001; Leichsenring et al., 2006; Menzies et al., 2002; Pasinelli and Brown, 2006; Shaw, 2005). Remarkably, the elevation of reactive oxygen species (ROS) leading to oxidative stress are shown to be associated with mitochondrial dysfunction (Barber et al., 2006; Menzies et al., 2002) and abnormal accumulation of neurofilaments in neurons (Kim et al., 2004). Further, ROS induces the disruption of glutamate uptake via glutamate transporter (EAAT2) in astrocytes, which is implicating in excitotoxic neuronal cell death (Rao et al., 2003; Rao and Weiss, 2004; Trotti et al., 1999). Thus, oxidative stress appears to play a central role in the pathogenesis for ALS.

Recently, we have identified L-745,870 as a neuronal apoptosis inhibitory protein (NAIP/BIRC1)-upregulating compound (Okada et al., 2005). NAIP is a member of the inhibitor of apoptosis protein (IAP) family and is known to exert potent protective activity against oxidative stress-induced cell death (Liston et al., 1996). In fact, although it has originally reported that L-745,870 acts as an antagonist for the dopamine D4 receptor (Patel et al., 1997), we found that L-745,870 selectively inhibited oxidative stress-induced cell death *in vitro* (Okada

* Corresponding author. Neurodegenerative Diseases Research Centre, Graduate School of Medicine, Tokai University Isehara, Kanagawa 259-1193, Japan. Fax: +81 463 91 4993.
E-mail address: jeikeda3@is.icc.u-tokai.ac.jp (J.-E. Ikeda).

0014-4886/$ – see front matter